Apoptosis (2022) 27:261–282
https://doi.org/10.1007/s10495-022-01711-6

# Piperlongumine, a piper alkaloid, enhances the efficacy of doxorubicin in breast cancer: involvement of glucose import, ROS, NF-κB and lncRNAs

**Nikee Awasthee[1] · Anusmita Shekher[1] · Vipin Rai[1] · Sumit S. Verma[1] · Shruti Mishra[1] · Anupam Dhasmana[2,3] · Subash C. Gupta[1,4]**

Accepted: 8 January 2022 / Published online: 4 February 2022


## Abstract

Piperlongumine (PL, piplartine) is an alkaloid derived from the *Piper longum* L. (long pepper) roots. Originally discovered in 1961, the biological activities of this molecule against some cancer types was reported during the last decade. Whether PL can synergize with doxorubicin and the underlying mechanism in breast cancer remains elusive. Herein, we report the activities of PL in numerous breast cancer cell lines. PL reduced the migration and colony formation by cancer cells. An enhancement in the sub-G1 population, reduction in the mitochondrial membrane potential, chromatin condensation, DNA laddering and suppression in the cell survival proteins was observed by the alkaloid. Further, PL induced ROS generation in breast cancer cells. While TNF-α induced p65 nuclear translocation, PL suppressed the translocation in cancer cells. The expression of lncRNAs such as MEG3, GAS5 and H19 were also modulated by the alkaloid. The molecular docking studies revealed that PL can interact with both p65 and p50 subunits. PL reduced the glucose import and altered the pH of the medium towards the alkaline side. PL also suppressed the expression of glucose and lactate transporter in breast cancer cells. In tumor bearing mouse model, PL was found to synergize with doxorubicin and reduced the size, volume and weight of the tumor. Overall, the effects of doxorubicin in cancer cells are enhanced by PL. The modulation of glucose import, NF-κB activation and lncRNAs expression may have contributory role for the activities of PL in breast cancer.

**Keywords** Alkaloid · Chemoresistance · LncRNA · NF-κB · Piperlongumine · Warburg effect

## Introduction

Many solid tumors including breast cancer heavily depend on glycolysis even in the presence of oxygen to meet their energetic demands. In the process, lactic acid is produced inside the cells. This phenomenon *i.e.* preferential use of aerobic glycolysis is known as the Warburg effect [1]. The increased transport of glucose through the glucose transporters (GLUTs) is the characteristics of Warburg effect [2]. Seven members of GLUT family (GLUT1-6 and GLUT12) are overexpressed in breast cancer. GLUT-1 level is elevated in higher grade and poorly differentiated breast tumors [3]. The GLUT-1 level also correlates with high proliferation rates and aggressiveness of breast cancer [3]. On the other hand, transporters such as MCT4 facilitate lactate efflux from highly glycolytic cells [4]. The Warburg effect is crucial for tumorigenesis and thus could be considered as a novel avenue for the therapeutics development. Whereas oncogenes are reported to promote, the tumor suppressors reduce the Warburg effect. Recent studies suggest that the Warburg effect can also be modulated by the inflammatory molecules in the tumor microenvironment [5].

Nuclear factor kappa B (NF-κB) is required for GLUT-1 plasma membrane trafficking downstream of AKT [6]. NF-κB is a crucial regulator of energy homeostasis and

✉ Subash C. Gupta
sgupta@bhu.ac.in

1 Department of Biochemistry, Institute of Science, Banaras Hindu University, Varanasi 221 005, India

2 Department of Bioscience and Cancer Research Institute, Himalayan Institute of Medical Sciences, Swami Rama Himalayan University, Dehradun 248 016, India

3 Present Address: Department of Immunology and Microbiology, School of Medicine, University of Texas Rio Grande Valley, Edinburg, TX, USA

4 Department of Biochemistry, All India Institute of Medical Sciences, Guwahati, India

aerobic glycolysis in mouse embryonic fibroblasts [7]. RRAD, a tumor suppressor reduced the Warburg effect by negatively regulating GLUT1 translocation and NF-κB signaling in lung cancer cells [8]. IKKβ and NF-κB activated by α-ketoglutarate enhances glucose uptake and tumor cell survival by upregulating GLUT1 [9]. NF-κB is a pleiotropic molecule with a potential in the pathogenesis of multiple human ailments. Under normal conditions, NF-κB consists of p50, p65 and the inhibitory kappa B (IκB) subunits and resides in the cytoplasm. In the presence of activating stimulus, p65-p50 subunit dissociate from IκB, translocate into the nucleus and binds to DNA sequence activating target gene transcription [10].

The NF-κB signaling pathway is regulated by the protein coding genes. Additionally, this transcription factor can also be modulated by the long non-coding RNAs (lncRNAs) [11]. HOTAIR, lincRNA-p21, MALAT1, MIR31HG, NKILA and PACER are some of the NF-κB related lncRNAs [11]. Like NF-κB, lncRNAs can also regulate enzymes, molecules, and oncogenes associated with the glucose metabolism in cancer. For instance, LINC00504 can stimulate aerobic glycolysis by interacting with miR-1244 in ovarian cancer cells [12]. Similarly, glucose metabolism is regulated through mTOR-mediated translation of TCF7L2 in hepatocellular carcinoma [13]. The lncRNA, IDH1-AS1 activates the Warburg effect under normoxia through c-Myc and HIF1α [14]. Also, cancer cells can be sensitized to anti-cancer agents through the mediation of lncRNAs and NF-κB. The lncRNA NBR2 modulated the sensitivity of cancer cells to phenformin through GLUT1 [15]. An improvement in glucose uptake and aerobic glycolysis is associated with development of chemoresistance in multiple tumor types. The combination of chemotherapeutics with metabolic modulators could be a potential strategy to overcome drug resistance.

Chemotherapy, radiotherapy and surgery have been used for breast cancer. Yet, breast cancer constitutes the major cause of death in women globally. Piperlongumine (PL, piplartine) is an alkaloid derived from the roots of the ayurvedic plant, *Piper longum* L. (long pepper). Originally discovered in 1961 [16], the biological activities of this molecule were reported only during the last decade. The anti-cancer activities of PL was originally discovered in a search for anti-neoplastic drugs during a screening program of 5166 molecules between 2000 and 2007 [17]. The alkaloid exhibits activities against biliary cancer [18], gastric cancer [19], colon cancer [20], melanoma, multiple myeloma [21], NSCLC [22], pancreatic cancer [23], oral cancer [24], and prostate cancer [25]. At the molecular level, this alkaloid can modulate several cancer related targets such as phosphoinositide 3-kinases (PI3K)/AKT/mTOR pathway [26], NF-κB signalling [27], STAT3 signalling [28], caspase-3, B-cell lymphoma 2 (Bcl-2), PARP [29], and c-Jun NH2-terminal kinase [30]. PL is also known to inhibit glutathione S-transferase p (GSTp) and carbonyl reductase 1 (CBR1). This results in the disruption of redox homeostasis and ROS generation in cancer cells [31]. PL is also known to enhance the activities of 5-fluorouracil (5-FU), cisplatin, paclitaxel and curcumin in cancer cells. At sub-optimal concentration, PL is known to radio-sensitise MDA-MB-231 cells. The radiosensitization effects of PL is mediated partly through regulation of apoptosis-related proteins and ROS generation [32].

Although PL exhibit activities against some cancer types, its potential against breast cancer is poorly understood. The goal in this manuscript was to investigate if PL can modulate the sensitivity of cancer cells to doxorubicin. The modulatory role of PL on glucose metabolism was also examined. Finally, we evaluated if the anti-cancer activities of PL is associated with its modulatory effects on NF-κB activation and lncRNAs expression.

## Material and methods

### Reagents

PL was obtained from Sami Labs Limited (Bangalore, Karnataka). We procured doxorubicin hydrochloride from Tokyo Chemical Industry (Portland, Oregon). Trypsin, Dulbecco's modified Eagle's medium (DMEM), ethylenediaminetetraacetic acid (EDTA), streptomycin, and penicillin were procured from Himedia (Mumbai, Maharashtra). Crystal violet, dimethyl sulfoxide (DMSO), 3-[4,5-dimethylthiazol-2-yl]-2,5-diphenyl tetrazolium bromide (MTT), haematoxylin and eosin (HE) were obtained from SRL Diagnostics (Mumbai, Maharashtra). Acridine orange (AO), ethidium bromide (EtBr), 5, 5′, 6, 6′-Tetrachloro-1, 1′, 3, 3′-tetraethyl benzimidazolylcarbocyanineiodide (JC-1), 4′,6-diamidino-2-phenylindole (DAPI), propidium iodide (PI), agarose, 2′,7′-dichlorodihydrofluorescein diacetate ($H_2$DCFDA), fetal bovine serum (FBS), MitoTracker Red CMXRos, and Alexa Fluor 488 were obtained from Invitrogen (Carlsbad, California). TNF-α was obtained from Genentech (San Francisco, California). TRI Reagent was obtained from Sigma (Bengaluru, Karnataka). The p65 antibody was purchased from Abcam (Cambridge, UK). The glucose estimation kit was obtained from BEACON Diagnostics (Navsari, Gujarat) while triglyceride and cholesterol estimation kit were obtained from ARKRAY Healthcare (Surat, Gujarat). Antibodies against PARP and Bcl-2 were obtained from Santa Cruz Biotechnology (Santa Cruz, California). MMP-9 and PDL-1 antibodies were procured from Cell Signaling Technology (Danvers, Massachusetts) and proteintech (Rosemont, Illinois), respectively. The primers for H19, GAS5, MEG3, beta-2 microglobulin (B2M), 5S rRNA were procured from Eurofins Genomics (Bangalore, Karnataka). PCR

master mixture (SYBR green) was procured from Agilent Technologies (Foster City, California).

### Cell lines

MDA-MB-468, MDA-MB-231, MCF-7, T-47D (breast cancer cell lines) and EAC cells were purchased from National Centre for Cell Science, India. The high glucose DMEM was used to culture the cells. FBS (10%), penicillin (100 units/mL) and streptomycin (100 µg/mL) were added in the growth medium.

### Cytotoxicity, cell viability and cell proliferation assay

We evaluated the cytotoxicity in the presence of test agents by analysing the mitochondrial reductase activity-MTT assay [33]. MTT was used as a substrate. The results from MTT assay often correlate with the effects on the cell viability and the cell proliferation. The cells were seeded in various wells (10,000/well) and treated with different concentrations of test agents for 24 h, 48 h and 72 h. The cytotoxicity was measured at each time point. Thus, the ability of the cells to proliferate over the period of time was determined. The cytotoxic effects were determined by measuring the optical density of purple formazan at 570 nm.

### Determination of interaction between PL and doxorubicin

To determine the interaction between PL and doxorubicin, we used Chou-Talalay method [34]. MCF-7 cells were exposed with 1–100 µM PL for 24 h. After washing, the cells were exposed to 0.25–4 µM doxorubicin for another 24 h. The cytotoxicity was determined by measuring mitochondrial reductase activity. To define the type of effect, we calculated Combination Index (CI) using CompuSyn software (ComboSyn, Paramus, NJ, USA). We calculated CI for every fraction affected (fa) value. A value of 'percent inhibition/100' refers to 'fa'. The values of $CI > 1$, $CI < 1$ or $CI = 1$ indicated whether the drug interactions were antagonistic, synergistic or additive, respectively.

### Clonogenic assay

For this assay, we made minor changes in a previously published method [35]. We seeded cells (1000/well) in various wells overnight. Then, the cells were supplemented with fresh media containing 5–15 µM PL. After 24 h, the agents were washed off and the cells were left for colony formation. After 10 days, 0.25% crystal violet was used for staining the colonies. Finally, we counted the number of colonies in a manual manner.

### DNA laddering assay

For DNA laddering, we followed a widely accepted method with minor modifications [36]. The normal and exposed cells were washed with PBS and suspended in a buffer containing Tris–HCl (100 mM, pH 8.5), NaCl (5 M), EDTA (5 mM), and SDS (10%). Then, we subjected the lysate to proteinase K (20 mg/mL) at 55 °C (2 h) for partial deproteinization. The DNA was precipitated with isopropanol and chloroform. The DNA was then centrifuged at 12,000 rpm (4 °C) for 15 min. We used 70% ethanol to wash the DNA pellet. The pellet was finally dissolved in Tris–EDTA buffer after air drying. We used EtBr containing agarose gel (1.5%) for DNA electrophoresis. For visualization and capturing of the DNA bands, gel-doc system (BioRad Gel Doc XR +) was used.

### DAPI staining

The effects of PL on the nuclear structure was examined by DAPI staining [37]. We seeded the cells ($1 \times 10^6$) over coverslip for overnight. Then, the cells were exposed with various concentration of agents for 24 h. The cells were then PBS washed and fixed at room temperature with paraformaldehyde (15 min). Finally, the cells were permeabilized for 30 min with methanol at − 20 °C and stained with DAPI. We used fluorescence microscope to visualize the changes in the structure of nucleus.

### Viability assay by staining with acridine orange/propidium iodide (AO/PI)

PL mediated changes in the cell viability was evaluated by AO/PI double staining. Briefly, cells were treated with 1–15 µM PL (24 h), washed and stained with 100 µg/mL AO/PI. The cells were finally visualized under fluorescence microscope.

### Analysis for cell cycle distribution

The percent distribution in different phases of cell cycle in the normal and treated groups was evaluated by PI staining and flow cytometry [33]. The cells were exposed with multiple concentrations of PL. After washing with PBS, the cells were methanol fixed and stained with PI in the dark for 30 min. The intensity of PI-stained nuclear DNA was examined by FACScan. We used cell quest software (Becton Dickinson) to analyse population in different phases of cell cycle.

### Determination of mitochondrial membrane potential (MMP, ΔΨ)

We assessed the changes in the MMP using the fluorochrome JC-1 by a previously published procedure [38]. The normal and exposed cells were incubated in the dark with JC-1 (10 µg/mL) for 20 min at 37 °C. The cells were then visualized using the fluorescence microscope after washing with PBS. We imaged the same microscopic field under the red filter and green filter in a sequence. The red fluorescence represented the cells with intact mitochondria. The cells containing the depolarized mitochondria were indicated by green fluorescence. To examine the changes in the mitochondrial membrane potential, we also used MitoTracker Red CMXRos dye. MDA-MB-231 cells were treated with 1–10 µM PL (24 h), and stained with mitotracker (15 min) at 37 °C. The cells were washed twice with PBS and the images were captured under the fluorescence microscope.

### Western blotting

The expression of cancer related proteins in the normal and treated cells was examined by western blot analysis [39]. The whole cell lysate was prepared from the control and treated cells. The lysate was electrophoresed on SDS PAGE gel. The protein separated by electrophoresis was transferred from gel to the membrane. The expression of various target proteins was detected using Clarity Western Enhanced Chemiluminescence (ECL) Substrate (BioRad, United States).

### Immunocytochemistry

We performed immunocytochemical analysis to assess the potential of PL in modulating the expression of p65, cytochrome c, and GLUT-1 at the cellular level [40]. For p65 expression, the cells were pre-treated with PL before stimulation with TNF-α. For GLUT-1 and cytochrome c expression, cells were exposed to various concentration of PL. When the treatment period was over, cells were fixed, permeabilized and incubated with blocking solution. The fixed cells were treated with antibodies (primary and secondary in a sequential manner) before staining with DAPI. Finally, the cells were visualized and photographed under the fluorescence microscope.

### Cell migration assay

The wound healing assay was performed to assess the effects of PL on cancer cell migration. At 90% confluency, the monolayer cells were scratched in each well by sterile tip. The scratched monolayers were then treated with PL and cell debris were removed by washing. The size of the scratched area was evaluated after 0, 18 and 36 h under the phase contrast microscope. We used Image J software for calculating the healed area and the wound size at each time point.

### Soft-agar colony formation assay

We assessed the development of tumor in vitro using the method as described previously [41]. In brief, a stock solution of 1% agarose was prepared in autoclaved double distilled water. An equal volume of 1% agarose and 2 × DMEM were mixed together. From this mixture, 2 ml was poured in each well of 6 well plate and allowed to settle for 30 min. Thus, the total concentration of agarose in this layer (lower) was 0.5%. In parallel, 10,000 cells from control and treatment groups in 1.1 ml 2X DMEM media from each group were mixed with 0.4 ml of 1% agarose. The mixture (1.5 mL) containing 0.27% agarose and cells (10,000) were poured over 0.5% lower layer. The 0.27% agarose with cells (upper layer) was left to solidify for 30 min. Then, 1 ml of DMEM media was added on the top of upper layer. The cells in the agarose were incubated at 37 °C with 5% $CO_2$ for 20 days. The media of the plate was changed on every alternate day. The colonies were then visualized under phase contrast microscope, photographed and counted.

### Assay for the generation of ROS

To assess the intracellular production of ROS, we treated the cells with various concentrations of PL (1 h) before evaluating ROS using the membrane permeable dye 2′,7′-dichlorodihydrofluorescein diacetate (H2DCFDA). The level of ROS in stained cells was measured by Becton Dickinson flow cytometer (BD Biosciences, New Jersey). The analysis was carried out using Cell Quest software [42].

### Quantitative reverse transcription polymerase chain reaction (qRT-PCR)

Whether PL and TNF-α affect the lncRNA expression was examined by qRT-PCR using a previously published method [36]. The sequences of primers are provided in Table 1. TRI reagent was used for the isolation of total RNA from the normal and exposed cells. The method supplied by the manufacturer (Invitrogen) was used. For reverse transcription, we used a high-capacity cDNA synthesis kit. SYBR green PCR master mix and Applied Biosystem 7500 Real-Time system was used for qRT-PCR. The data analysis and fold change was done by CT method and $2^{-\Delta\Delta CT}$ method, respectively [43]. The data were normalized from the values of housekeeping genes (5S rRNA, B2M).

**Table 1** The sequences of the primers used for the quantitative RT-PCR

| Gene/lncRNA | Forward sequence (5′-3′) | Reverse sequence (5′-3′) |
|---|---|---|
| H19 | ATCGGTGCCTCAGCGTTCGG | CTGTCCTCGCCGTCACACCG |
| GAS5 | CTTCTGGGCTCAAGTGATCCT | TTGTGCCATGAGACTCCATCAG |
| MEG3 | CTGCCCATCTACACCTCACG | CTCTCCGCCGTCTGCGCTAGGGGCT |
| 5S rRNA | GGCCATACCACCCTGAACGC | CAGCACCCGGTATTCCCAGG |
| B2M | CAGCATCATGGAGGTTTGAA | TGGAGACAGCACTCAAAGTA |

## Computational analysis

Lipinski's rule of five and ADMET (absorption, distribution, metabolism, excretion and toxicity) [44] properties were examined to evaluate the drug like features of PL (Compound CID: 637858) and doxorubicin (Compound CID: 31703). Lipinski's rule of five [45] states that an orally active drug does not violate more than one of these criteria: (i) no more than 5 hydrogen bond donors, (ii) no more than 10 hydrogen bond acceptors, (iii) a molecular mass less than 500 daltons, and (iv) log $P < 5$. PubChem databases were employed for the SMILE IDs of PL and doxorubicin. The conversion of SMILE ID to pdb files was done from CORINA 3D server. The 3D structure of p65 (Chain A), p50 (Chain B), and IκBα (Chain E) were procured from PDB ID 1NFI. TAK-1 and IKKα were obtained from 2EVA and 5TQY, respectively. 3D crystal structure of GLUT1 (1NFI Chain A) was retrieved from the RCSB protein data bank. Crystal structure of NFKBIB was not available in RCSB. Therefore, NFKBIB was modelled using SPARKS-X server. The protein quality validation was done from Ramachandran plot (https://zlab.umassmed.edu/bu/rama/). The poses of ligands/proteins and binding affinities were identified using AutoDock tool 4 [46]. GeneMANIA was used for generating functional link hypotheses. ZDock server was used for identifying interactions between GLUT1 (SLC2A1) and NF-κB-p65 (RELA) [47].

## Animal studies

Eight-week-old female mice (Swiss Albino) with a weight of 22–25 g were obtained from the animal facility, Institute of Medical Sciences, Banaras Hindu University, Varanasi, India. Five mice were housed per cage in a room fixed at constant temperature (12 h light and dark cycle). A normal chow diet with water ad libitum was provided to the mice. The approval of the protocol was obtained from the Animal Ethics Committee of Banaras Hindu University. For animal studies, Ehrlich ascites carcinoma (EAC) cells ($1 \times 10^7$) were injected into the peritoneal cavity of mouse. Originated from mammary tissues, EAC is an undifferentiated carcinoma with high transplantable capability, no-regression, rapid proliferation, shorter life span, and 100% malignancy [48]. It does not have tumour specific transplantation antigen. After implantation, EAC cells were allowed to multiply. After 8–10 days, the cells were withdrawn from the peritoneal cavity of the mice, centrifuged and resuspended in PBS. Then, $1 \times 10^6$ EAC cells/0.1 mL PBS/animal was injected subcutaneously under the mammary fat pad. After tumor palpation was visible, mice were randomized into six groups (I) untreated control (0.9% NaCl, 0.1% DMSO solution); (II) PL (10 mg/kg); (III) Doxorubicin (1 mg/kg); (IV) PL (20 mg/kg); (V) Doxorubicin (2.5 mg/kg); (VI) PL (10 mg/kg) + Doxorubicin (1 mg/kg). PL and Doxorubicin was administered intraperitoneally (IP) at every alternate day for 21 days. DMSO was used for preparing the stock solution of PL and further dilution was done in 0.9% NaCl. Over the period of treatment, tumor volume, body weight and food intake by mice were estimated on a weekly basis. The tumor volume was measured by Vernier caliper using the formula $1/2 \times L \times W^2$ (L = tumor length, W = tumor width) [49]. After the treatment period was over, mice were euthanized, and the tumor and blood samples were collected. The tumor weight was also recorded. The blood was used for the determination of metabolic parameters. Hematoxylin and eosin staining was used for assessing the morphological changes in the excised tumors.

## Tumor histology

We performed histology to examine the morphological changes in the tumor of the mice. The tissues were first fixed in freshly prepared Bouin's fluid. The fixed tissues were dehydrated in graded ethanol, cleared in xylene, and embedded in paraffin in order to be sliced into 5–6 µm sections. Subsequently, the sections were deparaffinized, dehydrated and stained with hematoxylin and eosin. The stained tissues were mounted and examined using a light microscope.

## Measurement of glucose, triglyceride, cholesterol and pH

We estimated the pH and glucose concentration in the medium from control and treated cells. The cells were treated without or with PL. After 24 h, when the confluency was almost 70%, the pH of the medium was measured. The glucose concentration in the medium from the control and treated groups was estimated using glucose estimation kit

following the instructions as provided by the manufacturer. The glucose was also estimated in the serum of mice from the normal and PL treated groups [50]. We estimated the concentration of triglyceride and cholesterol in the serum of mice using specific kits.

### Statistical analysis

The analysis of various parameters in the control and the experimental groups was performed. The comparison between two groups were performed by unpaired Student's t test. The significance level was ascribed at a value of $P < 0.05$.

## Results

Our aim was to examine the potential of PL against breast cancer. Most experiments were performed in breast cancer cell lines. The efficacy of PL was also examined in tumor bearing mouse model. We determined the potential of PL in sensitizing breast cancer cells to doxorubicin. The modulatory effects of PL on the key cancer related targets such as NF-κB, lncRNAs, ROS, and tumorigenic proteins were examined. Whether PL modulate metabolic parameters in breast cancer were also examined.

### PL suppresses the TNF-α induced NF-κB activation and modulate the lncRNAs expression

TNF-α is one of the potent inducers of NF-κB. We evaluated the effects of PL on TNF-α induced NF-κB activation. We exposed the cells with PL and TNF-α alone or with PL followed by TNF-α. Using immunocytochemistry and specific antibody, we found that p65 is mostly located in the cytoplasm under normal conditions (Fig. 1A). Upon stimulation with TNF-α, an accumulation of p65 was observed in the nucleus of the cells. PL, alone was unable to affect cellular localization of p65. However, when cells were exposed to 10 µM PL prior to stimulation with TNF-α, the nuclear content of p65 was almost completely reduced. Overall, PL reduces TNF-α induced NF-κB activation in MDA-MB-231 cell lines.

Next, we examined if PL can interact with the proteins of NF-κB signalling using in silico tools. The binding energies (kcal/mol) of IκBα, IKKα, p50, p65 and TAK1 with PL were − 4.25, − 5.95, − 5.78, − 6.31 and − 6.48, respectively (Table 2). Ki (dissociation constant, µM) values of IκBα, IKKα, p50, p65 and TAK1 with PL were 772.81, 43.41, 57.79, 23.90 and 17.75, respectively. Furthermore, PL was found to interact with p65 and p50 subunits (Fig. 1B, C). Collectively, these results suggest that PL can interact with the proteins of NF-κB signalling.

Because lncRNAs are involved in the tumorigenesis, we evaluated the modulatory effects of PL on lncRNAs. MDA-MB-231 cells were exposed with 10 µM PL. After 24 h, total RNA was extracted, reverse transcribed and examined for lncRNAs by qRT-PCR. We observed an induction of 5.4 fold and 2.4 fold in the expression of GAS5 and MEG3 by 10 µM PL, respectively (Fig. 1D). Conversely, the expression of H19 was reduced by 0.46-fold after treatment with 10 µM PL. Overall, these results suggest the modulatory effects of PL on the lncRNAs expression pattern in MDA-MB-231 cell lines. We also observed an upregulation in the expression of H19 and a downregulation in the expression of MEG3 and GAS5 by TNFα (Supplementary Fig S1).

### PL reduces glucose import by breast cancer cells

Like other solid tumors, breast cancer is characterized by increased dependence on glycolysis for their metabolic demands. In the process, cancer cells consume large amount of glucose as compared to normal cells. While doing so, cancer cells produce lactic acid inside the cell, which is eventually taken out of the cells. This results in a drop in the extracellular pH leading to acidosis. We examined the extracellular glucose concentration using a glucose estimation kit. The MDA-MB-231 cells were exposed with 1–20 µM PL. The extracellular glucose was estimated after 24 h. We observed an increase in the extracellular glucose with an increase in PL concentration (Fig. 2A). Overall, the glucose import by the cancer cells is impaired after PL treatment. We also examined the extracellular pH in the culture media of the cells from control and experimental groups. The pH of the medium from the control group after 24 h of culture was in the range of 6.2–6.3 (Fig. 2B). However, the pH of the medium from the PL treated groups was found in the range of 6.8–7.1. Furthermore, the pH of the medium without cells was unaffected by the PL.

### PL exposure modifies the expression of glucose and lactate transporter in breast cancer cells

While GLUT-1 is required for glucose influx, MCT-4 facilitate lactic acid efflux. Because PL affected extracellular glucose and extracellular pH, whether this alkaloid can modulate the expression pattern of GLUT-1 and MCT-4 was examined. GLUT-1 expression was examined by immunocytochemistry in the normal and in the cells treated with 1–10 µM PL. The control cells expressed constitutive level of GLUT-1 (Fig. 2C). With an increase in the concentration of PL, a suppression in the level of GLUT-1 was observed. The level of GLUT-1 was almost completely suppressed at 10 µM PL. To confirm the observations obtained by immunocytochemistry, we

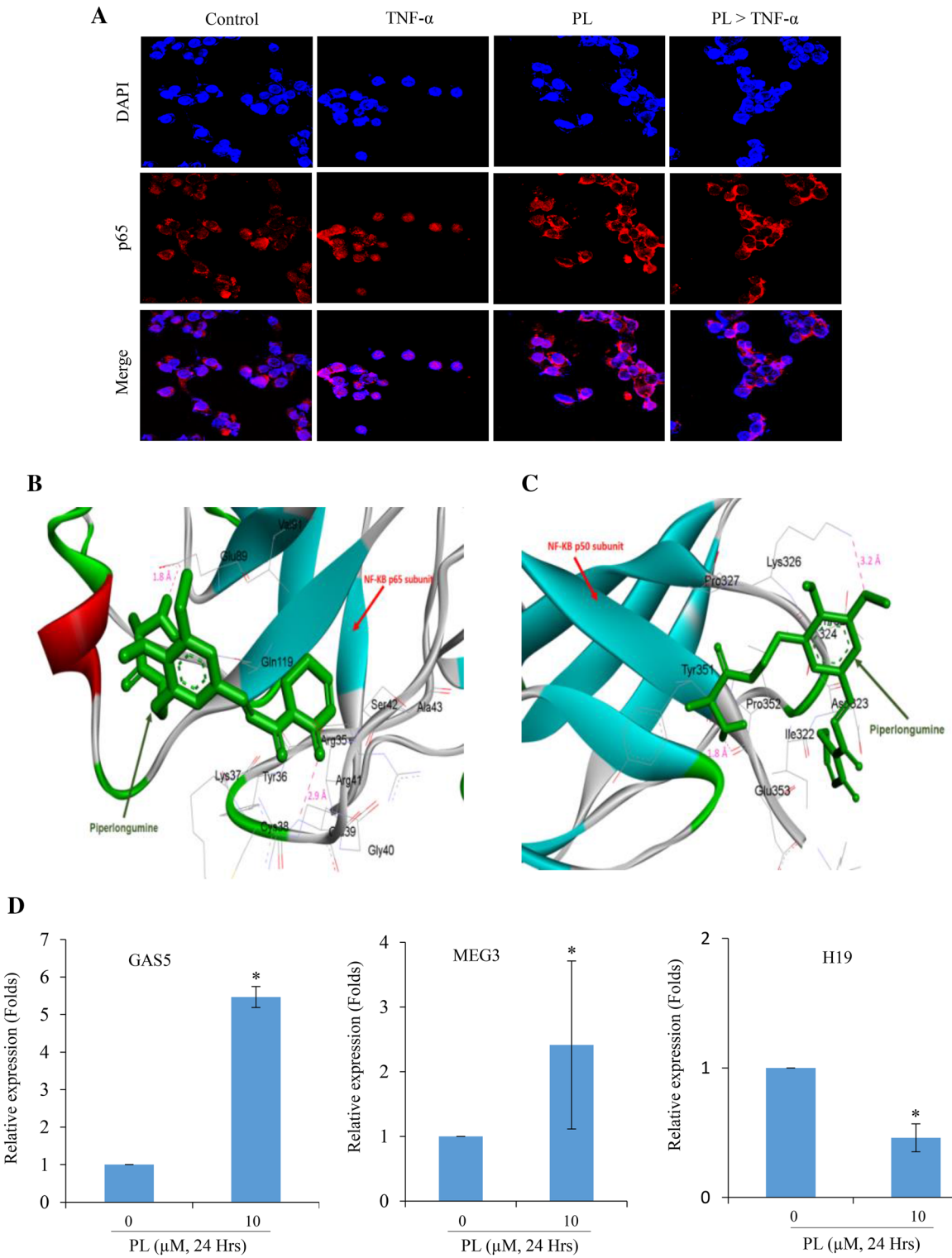


**Fig. 1** PL suppresses TNF-α induced NF-κB activation and modulate the expression of lncRNAs in breast cancer cells. **A** MDA-MB-231 cells were exposed with 10 μM PL for 6 h. Cells were then washed and treated with 1 nM TNF-α for 1 h. The cellular localization of p65 was determined by immunocytochemistry. **B**, **C** Molecular docking for the physical association of PL with p65 and p50. **D** MDA-MB-231 cells were exposed with 10 μM PL for 24 h. The quantitative RT-PCR was employed for examining the expression of lncRNAs. 5S rRNA was used as internal control. Where shown, the values are mean ± SE from three replicates. *shows the significance level as compared to control; $P < 0.05$. *PL* piperlongumine

**Table 2** Molecular docking analysis of piperlongumine with major proteins of NF-κB signaling pathway and GLUT-1

| Receptor | Binding Energy (kcal/mol) | Ki (μM) | Binding residues | H-Bonds | Distance (Å) |
|---|---|---|---|---|---|
| IκBα (1NFI Chain E) | − 4.25 | 772.81 | Arg143, Glu153, Gln154, His184, Ile192, His193, Leu227 | UNK1:H31-E:Glu153:OE2<br>UNK1:H32-E:Glu153:OE2 | 2.10663<br>2.15546 |
| IKKα (5TQY) | − 5.95 | 43.41 | Glu56, Arg57, Gly175, Glu176, Leu177, Cys178, Thr179, Glu180, Asn195, Tyr198 | UNK1:H31-A:Glu56:OE2<br>UNK1:H32-A:Glu56:OE1<br>UNK1:H32-A:Glu56:OE2 | 2.14824<br>1.89589<br>2.47747 |
| p50 (1NFI Chain B) | − 5.78 | 57.79 | Ile322, Asn323, Ile324, Thr325, Lys326, Pro327, Tyr351, Pro352, Glu353, Lys355 | B:Lys326:NZ-UNK1:O18<br>UNK1:H31-B:Pro352:O | 3.20458<br>1.80671 |
| p65 (1NFI Chain A) | − 6.31 | 23.90 | Arg35, Tyr36, Lys37, Cys38, Glu39, Gly40, Arg41, Ser42, Ala43, Glu89, Val91, Gln119 | A:Glu39:N-UNK1:O30<br>UNK1:H32-A:Glu89:OE2 | 2.96673<br>1.83138 |
| TAK1 (2EVA) | − 6.48 | 17.75 | Val42, Gly45, Ala46, Val50, Ser111, Tyr113, Asn114, Asp156, Lys158, Pro160, Asn161, Cys174, Asp175, Gly191 | A:Lys158:NZ-UNK1:O23<br>A:Gly191:N-UNK1:O30<br>UNK1:H31-A:Pro160:O<br>UNK1:H32-A:Asp175:OD2 | 2.75607<br>2.94518<br>2.10036<br>2.12881 |
| GLUT-1 (4PYP) | − 7.58 | 2.77 | Phe26, Ser80, Val83, Thr137, Gly138, Gln161, Ile164, Gln282, Gln283, Asn288, Phe379, Glu380, Gly384, Trp388, Ile404, Gly408, Asn411, Trp412, Asn415 | A:TRP388:HE1 -:UNK1:O9<br>A:ASN415:HD21 -:UNK1:O18<br>A:GLU380:OE1 -:UNK1:H32 | 1.9252<br>2.44866<br>2.4602 |

performed western blot analysis. A constitutive level of GLUT-1 was observed in control cells (Fig. 2D). The exposure of cells to PL was found to suppress GLUT-1 expression. For instance, the level of GLUT-1 was reduced to 0.6 and 0.2 fold at 5 μM and 15 μM PL, respectively. We also examined MCT-4 expression in normal and PL exposed cells. A constitutive level of MCT-4 was observed in control cells (Fig. 2D). PL suppressed MCT-4 expression in a concentration dependent manner. For instance, a respective 0.3 fold and 0.7 fold suppression in the level of MCT-4 was observed by 5 μM and 15 μM PL. Overall, PL can modulate the expression of GLUT-1 and MCT-4 in cancer cells. Next, we evaluated if PL can interact with GLUT-1 using computational tools. The binding energy and Ki values of GLUT-1 were observed to be − 7.58 kcal/mol and 2.77 μM, respectively (Table 2). Further, PL interacted with GLUT-1 through multiple amino acid residues (Supplementary Fig S2A). We used GeneMANIA to examine if GLUT-1 (SLC2A1) can interact with NF-κB p65 (RELA). SLC2A1 interacted with RELA through NFKBIB (Supplementary Fig S2B). PL was shown to exhibit preferential binding towards GLUT-1 than NF-κB-p65 and NFKBIB. Using ZDock server, we observed that NFKBIB and GLUT-1 interacted with 2606.585 zdock score in normal condition. After interaction of PL with GLUT-1, the protein binding score was decreased to 2567.608. This result indicated that PL has tendency to create a hindrance between GLUT-1 and NFKBIB.

## PL exhibits drug like properties

We performed in silico analysis to evaluate the molecular and drug like properties of PL along with doxorubicin, which is a widely used drug against breast cancer. PL and doxorubicin exhibited diverse characteristics as examined by Lipinski's rule of five (Table 3) and ADMET analysis (Table 4). The molecular weight, number of hydrogen bond acceptor, hydrogen bond donor and rotatable bonds for PL was found to be 317.34, 6, 0, and 5, respectively (Table 3). Thus, PL followed the Lipinski's rule of five. However, doxorubicin did not follow the Lipinski's rule of five as the molecular weight and the number of hydrogen bond acceptor was found to be 543.52 and 12, respectively (Table 3). ADMET analysis revealed the permeability of PL to blood brain barrier and human intestine. Further, no evidence of carcinogenicity and genotoxicity was observed (Table 4). Conversely, doxorubicin did not exhibit blood brain barrier and human intestine permeability. Furthermore, doxorubicin exhibited genotoxicity effects without any carcinogenicity.

Because PL exhibited drug like properties, we examined its cytotoxic effects by MTT assay. The cytotoxicity was examined over the period of time. The cytotoxicity data often correlates with cell viability and proliferation. The breast cancer cell lines were exposed to 0.1–100 μM PL. After an incubation of 24–72 h, the mitochondrial reductase activity was determined. The cytotoxic effects were increased by increasing the concentration (Fig. 3) and exposure time (Supplementary Fig S3). For instance, the

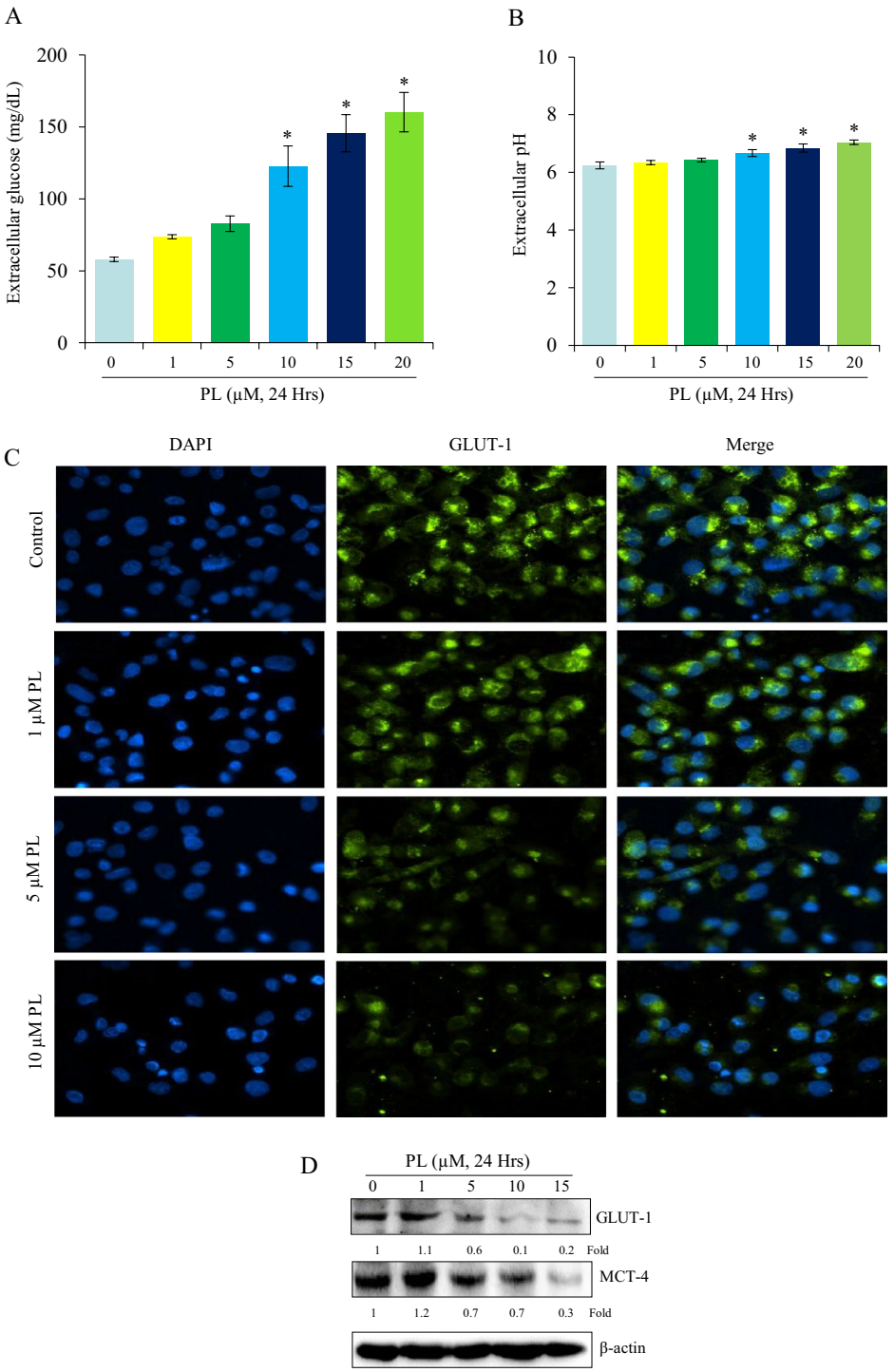


**Fig. 2** PL modulates glucose import and extracellular pH in cancer cells. **A** MDA-MB-231 cell lines were treated with 1–20 µM PL (24 h) and extracellular glucose was estimated using glucose estimation kit. **B** The pH of the medium from the control and treated groups were measured. **C** MDA-MB-231 cells were exposed with 1–10 µM PL (24 h). Immunocytochemistry was performed using a mouse monoclonal GLUT-1 antibody along with Alexafluor 488 conjugated mouse secondary antibody. The nuclei were then stained with DAPI and photographed under the fluorescence microscope. **D** MDA-MB-231 cells were treated with 1–15 µM PL (24 h). The whole cell extract was prepared and used for GLUT-1 and MCT-4 expression by western blot analysis. The data was normalized using β-Actin as a control. Where shown, the values are mean ± SD from three replicates. *indicate the significance level in comparison to control; $P < 0.05$. *PL* piperlongumine

**Table 3** Lipinski's rule of five for piperlongumine and doxorubicin

| Lipinski's feature | Piperlongumine | Doxorubicin |
|---|---|---|
| Molecular Weight | 317.34 | 543.52 |
| Number of hydrogen bond acceptor | 6 | 12 |
| Number of hydrogen bond donor | 0 | 7 |
| Number of rotatable bonds | 5 | 5 |

cytotoxicity was increased from 16.8 to 78.8% when MDA-MB-468 cells were exposed to 0.1 µM and 100 µM PL for 72 h, respectively (Fig. 3D). At 25 µM PL, the cytotoxicity of MDA-MB-468 cells was found at 36.2% and 52.5% after 24 h and 72 h, respectively (Supplementary Fig S3D). Further, the breast cancer cells responded to PL at varied levels. For instance, at 10 µM PL after 24 h, a respective 21%, 29.5%, 37.3% and 36.1% increase in the cytotoxicity was observed in MCF-7, T-47D, MDA-MB-468, and in MDA-MB-231 cells. Overall, PL affects the breast cancer cells proliferation irrespective of cell type. Further, breast cancer cells exhibit different levels of sensitivity to PL.

## PL reduces the colony formation of cancer cells

We performed clonogenic assay to assess the effects of PL on the colony formation of breast cancer cells. Using this assay, the ability of a cell for unlimited division and to form colonies can be examined. Cells were exposed with 5–20 µM PL for 6 h. Cells were then washed to remove the agent, left for colony formation for 10 days and stained with crystal violet. We counted the colonies in a manual manner. PL suppressed the colony number in a concentration dependent manner (Fig. 4A, B). At a concentration as minimum as 5 µM, the colony formation was drastically reduced. At 20 µM PL, no colonies were observed. MDA-MB-231 cells were more sensitive to PL as compared to MCF-7 cells. For example, at 10 µM PL, a respective 33.5% and 64.3% reduction in the colony formation was found in MCF-7 cells and MDA-MB-231 cells.

Many cell types adhere to the extracellular matrix for survival and proliferation. The transformed cells can proliferate in suspension without any support of the matrix. This type of proliferation is termed anchorage independent growth and mimics with tumorigenic potential in vivo. We also performed a soft agar colony formation assay. MDA-MB-231 cells were exposed to 1–20 µM PL for 24 h. The control and treated cells (10,000 per group) were suspended in soft agar (0.27%) in growth medium containing FBS. The suspended cells were then evenly distributed onto slightly solid hard agar (0.5%) containing medium and FBS. The cells poured on to the solid hard agar were kept in $CO_2$ incubator for 20 days. The fresh growth medium was added onto agar plates every alternate day for replenishing media and

**Table 4** In silico ADMET analysis of piperlongumine and doxorubicin

| Ligand | Absorption | | Metabolism | | | | | | | | | Excretion | Toxicity | |
|---|---|---|---|---|---|---|---|---|---|---|---|---|---|---|
| | BBB | HIA | P-Glycoprotein | | CYP-450 substrate | | | CYP-450 inhibitor | | | | | | |
| | | | Pg-S | Pg-I | 1/2 | 2C9 | 2D6 | 3A4 | 1A2 | 2C9 | 2D6 | 2C19 | 3A4 | ROCT | AMES | Carcinogen |
| Piperlongumine [Compound CID: 637,858; SMIL ID: COC1 = CC(=CC(=C1OC)OC)C = CC(=O)N2CCC = CC2 = O] | + | + | + | +/+ | | – | – | + | + | – | – | – | – | – | – | – |
| Doxorubicin [Compound CID: 31,703; SMIL ID: CC1C(C(CC(O1)OC2CC(CC3 = C2C(= C4C(= C3O) C(= O)C5 = C(C4 = O)C(= CC = C5)OC)O)(C(= O)CO)O)N)O] | – | – | + | –/– | | – | – | + | – | – | – | – | – | + | – | – |

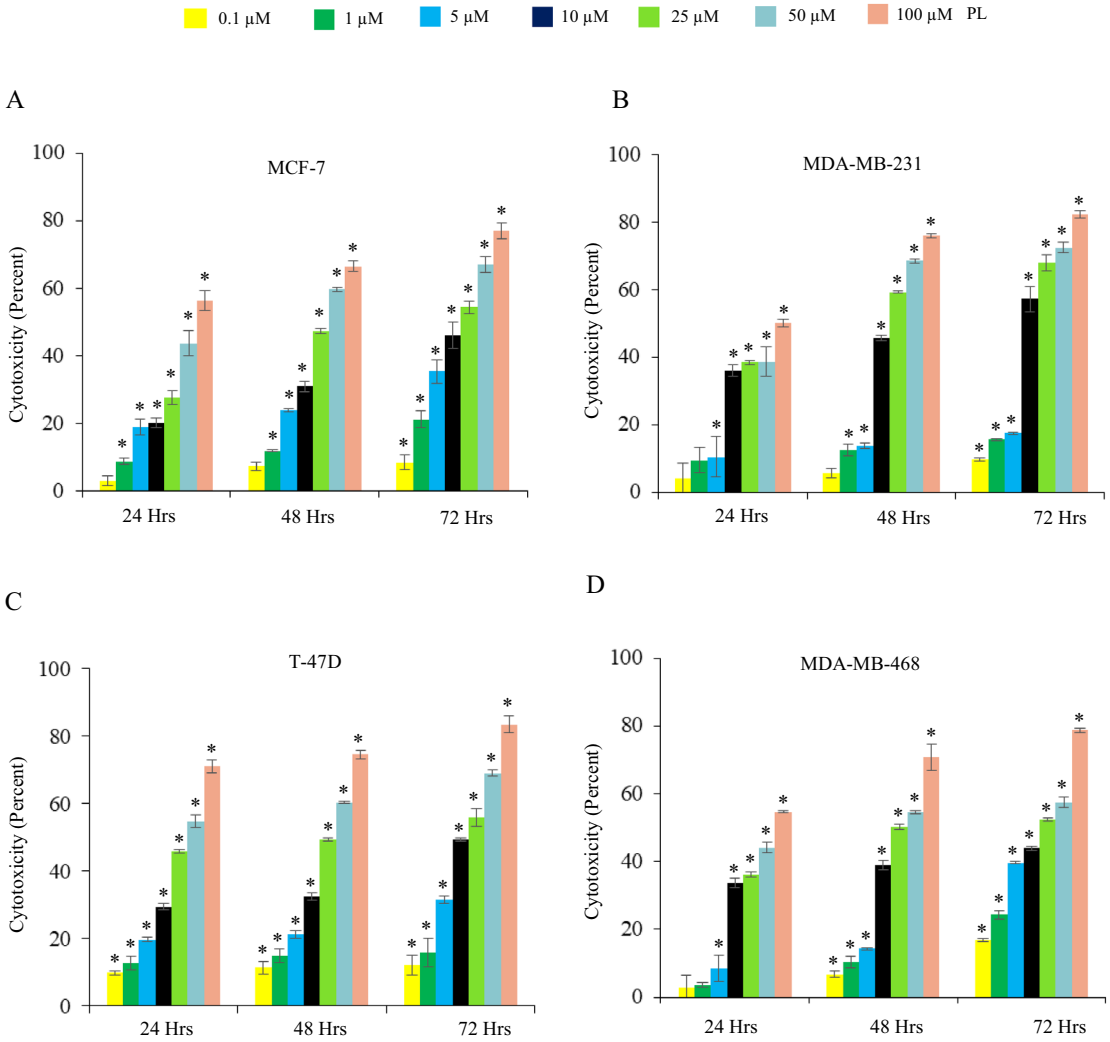


**Fig. 3** PL induces cytotoxicity in breast cancer cells. The cells were treated with 0.1–100 µM PL for 24–72 h. The mitochondrial reductase activity was determined by measuring the optical density at 570 nm. The data shown are mean ± SE from three replicates. *indicates the significance level as compared to untreated group; $P < 0.05$. *PL* piperlongumine

preventing the plates from drying out. Upon completion of the experiment, colonies were visualized and photographed. A high number of colonies were found in the untreated group (Fig. 4C). In the treatment group, the number of colonies were reduced with an increase in the concentration of PL. These results confirm the reducing effects of PL on the colony formation of breast cancer cells.

## PL triggers apoptosis in breast cancer cells

Apoptosis is a growth limiting regulatory mechanism by which cells trigger their own death in a designed manner. The tumor cells are reported to have impaired apoptotic pathways. One strategy for cancer therapy is to selectively stimulate tumor cells for apoptosis. Depending upon the severity of the stimuli, apoptosis can be at early-, mid- or late-stage. The ability of PL in triggering apoptosis was examined by AO/PI dual staining, DAPI staining, and DNA laddering. We assessed the effects of PL on the cell morphology by AO/PI dual staining. The percentage of apoptotic (early/late) and necrotic cells after PL treatment was also examined. AO and PI are dyes that bind to the nucleic acid. AO can stain both dead and live cells and results in green fluorescence. Only dead cells can take PI generating red fluorescence. The increase in PL concentration was accompanied with a reduction in the population of live cells and an increase in the population of apoptotic cells (Fig. 5A, Supplementary Fig S4A). The nuclear condensation and membrane blebbing, features of early apoptosis was found in both MCF-7 (Fig. 5A) and MDA-MB-231 (Supplementary Fig S4A) cells after PL treatment. In control cells, green intact nuclei were observed.

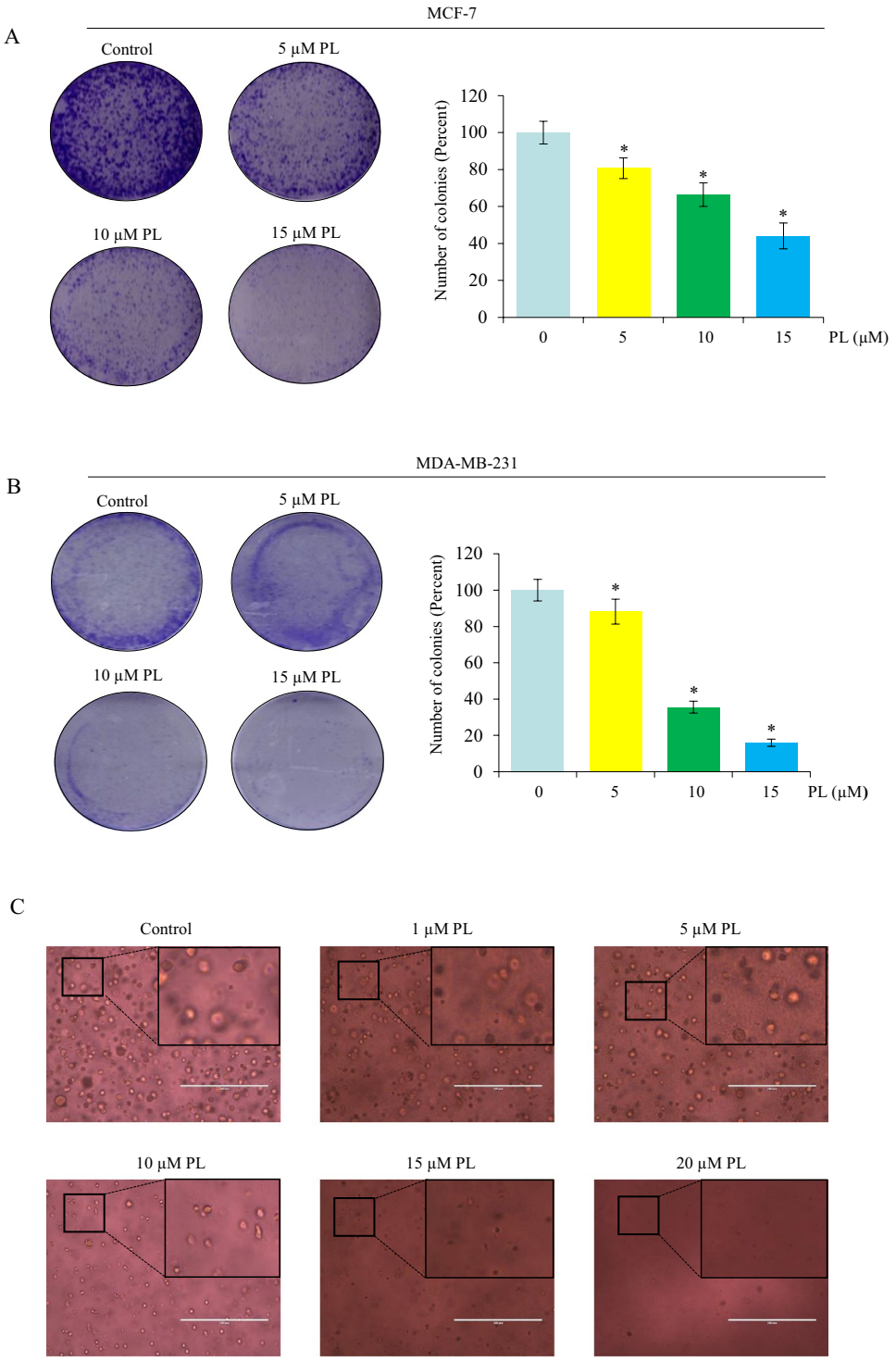


**Fig. 4** PL reduces the colony formation of cancer cells. **A** MCF-7 and **B** MDA-MB-231 cells were exposed with 5–20 µM PL for 6 h. After washing, the cells were left for colony formation for 10 days. The colonies were stained with crystal violet and counted manually. **C** MDA-MB-231 cells were exposed with 1–20 µM PL for 24 h and suspended in soft agar (0.27%) in 2 × DMEM growth medium. The suspended cells were evenly distributed onto slightly solid hard agar (0.5%) containing growth medium and placed in $CO_2$ incubator for 20 days. The fresh growth medium was added onto agar plates every alternate day to replenish the media and prevent the plates from drying out. At the end of the experiment, colonies were visualized using inverted phase contrast microscope. Where shown, the values are mean ± SD from three replicates. *indicate the significance level as compared to the untreated group. $P < 0.05$. *PL* piperlongumine

Whether PL affects the cell cycle distribution was examined in MDA-MB-231 cells. PI was used for staining the normal and exposed cells before analysis by flow cytometer. The increase in the PL concentration was found to increase the sub-G1 population (Fig. 5B). For example, the sub-G1 population was obtained at a respective 0.71%, 0.82%, 9.73%, and 15.68% by 1 µM, 5 µM, 10 µM, and 15 µM PL. During the late stages of apoptosis, fragmentation in DNA is observed. Whether PL can induce DNA fragmentation in cancer cells was examined. MDA-MB-231 cells were exposed to 2.5–20 µM PL for 24 h, DNA was isolated and separated on agarose gel. The DNA laddering and smearing pattern was observed at and above 10 µM PL (Fig. 5C). In control cells and at lower concentrations, DNA laddering

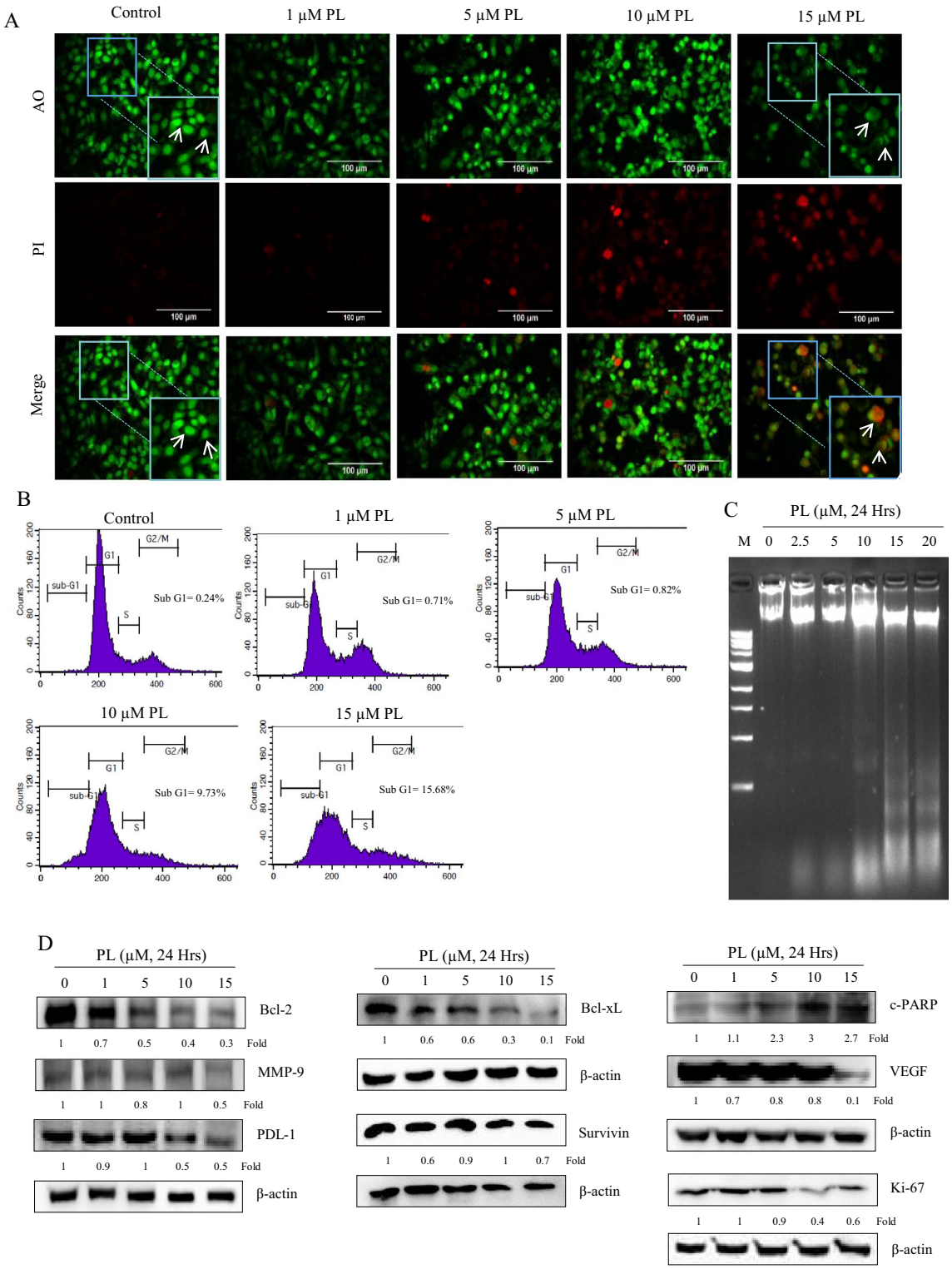


**Fig. 5** PL triggers apoptosis in breast cancer cells. **A** MCF-7 cells were exposed with 1–15 µM PL for 24 h. Then, the cells were stained with 100 µg/mL acridine orange/propidium iodide. The cells were washed and photographed under the fluorescence microscope. The nuclear condensation and membrane blebbing in the treated cells, and intact nuclei in the control cells are shown by arrows. **B** MDA-MB-231 cells were treated with 1–15 µM PL for 24 h. After fixation and PBS washing, the cells were stained with propidium iodide (1 mg/mL). The population at different phases was analyzed by flow cytometry. **C** MDA-MB-231 cells were treated with 2.5–20 µM PL for 24 h. The DNA was extracted and separated by electrophoresis on agarose gel. **D** MDA-MB-231 cells were exposed to 1–15 µM PL for 24 h. The western blotting was performed using the whole cell extract for the expression of proteins. The data was normalized using β-Actin as control. *PL* piperlongumine

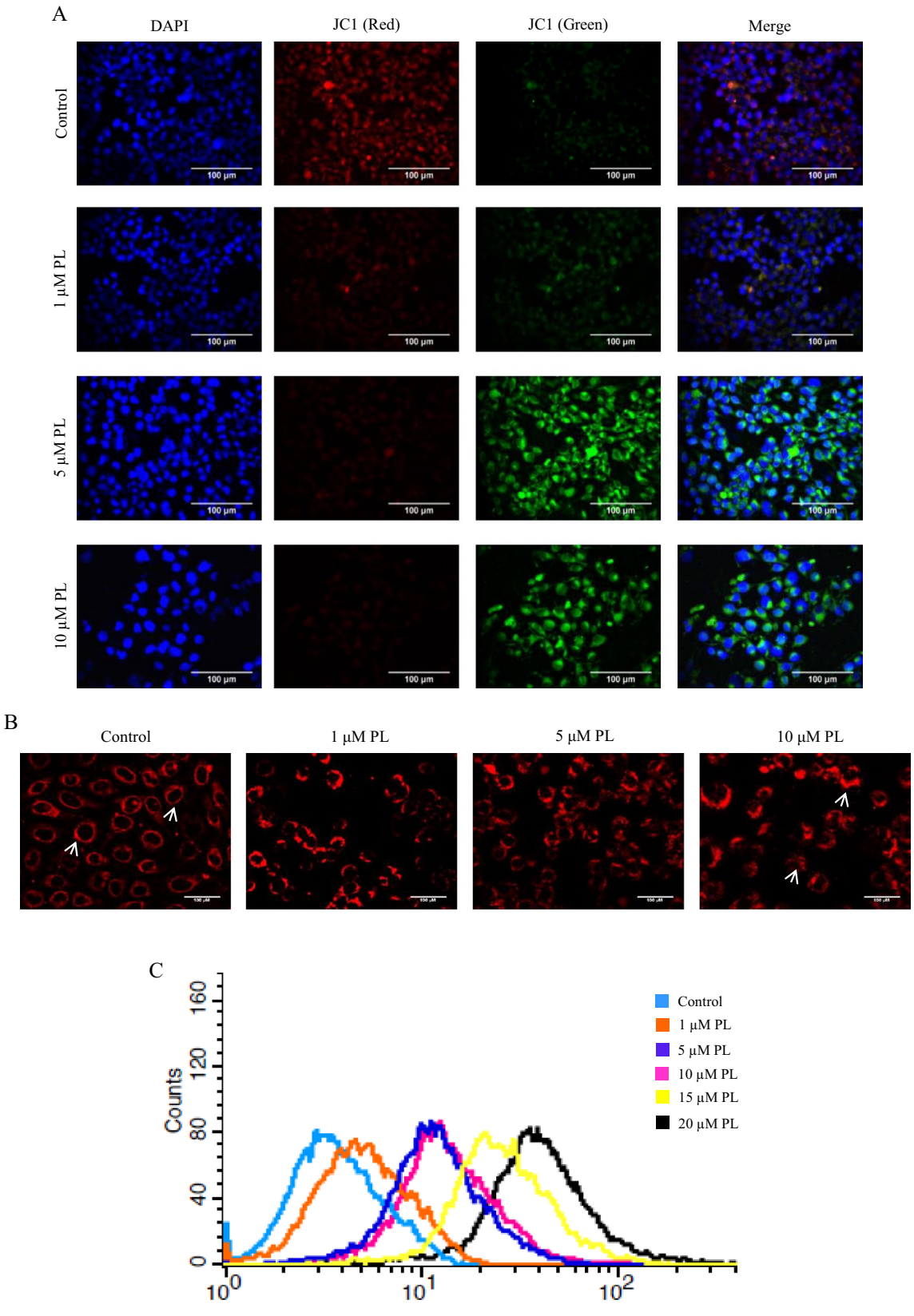
A
DAPI
JC1 (Red)
JC1 (Green)
Merge
Control
1 μM PL
5 μM PL
10 μM PL
100 μm
B
Control
1 μM PL
5 μM PL
10 μM PL
C
Counts
0
40
80
120
160
$10^0$
$10^1$
$10^2$
Control
1 μM PL
5 μM PL
10 μM PL
15 μM PL
20 μM PL

◂**Fig. 6** PL induces depolarization in mitochondrial membrane potential and ROS generation in cancer cells. **A** MDA-MB-231 cells were exposed with 1–10 μM PL for 24 h. The cells were incubated with JC-1 dye (10 μg/mL) and imaging was performed under fluorescence microscope. **B** MDA-MB-231 cells were exposed to indicated concentrations of PL for 24 h. The cells were then stained with 50 nM Mitotracker red and visualized under the fluorescence microscope. Arrows indicate the presence of intact mitochondria and fragmented mitochondria in the control and treated cells, respectively. **C** MDA-MB-231 cells were exposed with 1–20 μM PL (1 h) and stained with 10 μM $H_2$DCFDA (30 min). The ROS level was estimated by flow cytometry. *PL* piperlongumine

or smearing pattern was not observed. Whether PL effects the nuclear structure was also examined by staining with DAPI. Chromatin condensation and nuclear fragmentation was evident in the PL treated cells at 15 μM concentration (Supplementary Fig S4B). The normal shaped nuclei (oval or round) were observed in control cells. Further, the nuclear structure was unaffected at lower concentration of PL.

Whether PL can modulate the expression of tumorigenic protein in cancer cells was examined. The proteins related with anti-apoptosis (Bcl-2, Bcl-xL, Survivin), proliferation (Ki-67), invasion (MMP-9), and angiogenesis (VEGF) were constitutively expressed in control cells (Fig. 5D). However, these proteins were suppressed after the treatment with PL. For example, the expression of Bcl-2, Bcl-xL, Survivin and Ki67 was suppressed to 0.3, 0.1, 0.7, and 0.6 fold when cells were treated with 15 μM PL as compared to the untreated group. The expression of MMP-9 and VEGF was reduced to a respective 0.5 fold and 0.1 fold by 15 μM PL. The alkaloid also induced PARP cleavage in cancer cells. Programmed death-ligand 1 (PDL1), a 40 kDa type 1 transmembrane protein is often overexpressed in cancer cells. An upregulation in PDL1 allows cancer cells to evade the host immune system. We observed an abundance in the expression of PDL1 in the control cells. However, the treatment of cells with PL was found to suppress the expression of PDL1. Overall, the expression of cancer related proteins is modulated by PL in breast cancer cells.

## PL induces depolarization in the mitochondrial membrane potential (MMP) and ROS level in breast cancer cells

The early phases of apoptosis is characterized by an irreversible reduction in the MMP (ΔΨ). The effects of PL on the polarization of MMP was examined. For this, we used the JC-1, which is accumulated in the mitochondria in a potential-dependent manner. At lower membrane potential, green fluorescence is obtained from the JC-1 monomer. In cells with healthy mitochondria, JC-1 exist in the aggregated form and produces red to orange fluorescence. The control cells produced red fluorescence (Fig. 6A). After treatment with PL, cells with green fluorescence were observed. MitoTracker Red CMXRos is a dye that stains intact mitochondria but diffuses out when the membrane potential drops. We observed prominent staining in the normal MDA-MB-231 cells indicating an intact mitochondria (Fig. 6B). However, exposure of cells to PL was associated with a fragmentation in the mitochondria. Of note, the staining pattern of cytochrome c was detected in the mitochondria of control cells. After treatment with PL, reduction in the cytochrome c staining and cell shrinkage was observed. This suggested the release of the cytochrome c into the cytosol (Supplementary Fig S5). ROS generated inside the body under normal conditions is also implicated in several pathological conditions. Because ROS generation is one of the mechanisms for the activities of many cancer drugs, whether PL can induce ROS level in cancer cells was determined. For this, $H_2$DCFDA which is a cell permeable relatively nonfluorescent molecule was used. DCFH-DA is oxidized intracellularly by ROS to a fluorescent molecule, DCF. An increase in fluorescence intensity that represents DCF content is assumed to be proportional to intracellular ROS. MDA-MB-231 cells were exposed with 1–20 μM PL for 1 h and stained with $H_2$DCFDA. The fluorescence intensity representing the ROS level was evaluated by flow cytometry. The ROS level in the control group and in the 1 μM PL treated cells was minimal (Fig. 6C). However, a significant increase in the ROS level was observed with an increase in the concentration of PL. More specifically, a respective 3.2-fold, 3.7-fold, sevenfold and 10.8 fold induction in the ROS level was found at 5 μM, 10 μM, 15 μM, and 20 μM PL. Overall, PL reduces the MMP and enhances ROS level in breast cancer cells.

## PL reduces migration and sensitizes the breast cancer cells to doxorubicin

Metastasis is the major cause of the breast cancer deaths. The cancer cells migrate and invade before distant metastasis. The wound healing assay was carried out to examine the effect of PL on the cell motility. The motility of normal and PL treated MDA-MB-231 cells was examined at 0 h, 18 h, and 36 h. In the control cells, a respective 58.2% and 28.3% of the original wound size was observed after 18 h and 36 h (Fig. 7A). After treatment with 5 μM and 10 μM PL, the wound area was minimally occupied. For example, at 5 μM PL, the wound size was reduced to 73.7% and 46.9% after 18 h and 36 h, respectively (Fig. 7B). At 10 μM PL, the wound size was suppressed to 84.6% and 81.6% after 18 h and 36 h, respectively. We also calculated the healed area in the normal and exposed cells. The rise in the percent of occupied area over time in the untreated group was much higher in comparison to that observed in the treated group. For example, the healed area in the control group was observed at 78.5% after 36 h. On the other hand, the healed area was observed at 17.8% after 36 h in the group of cells

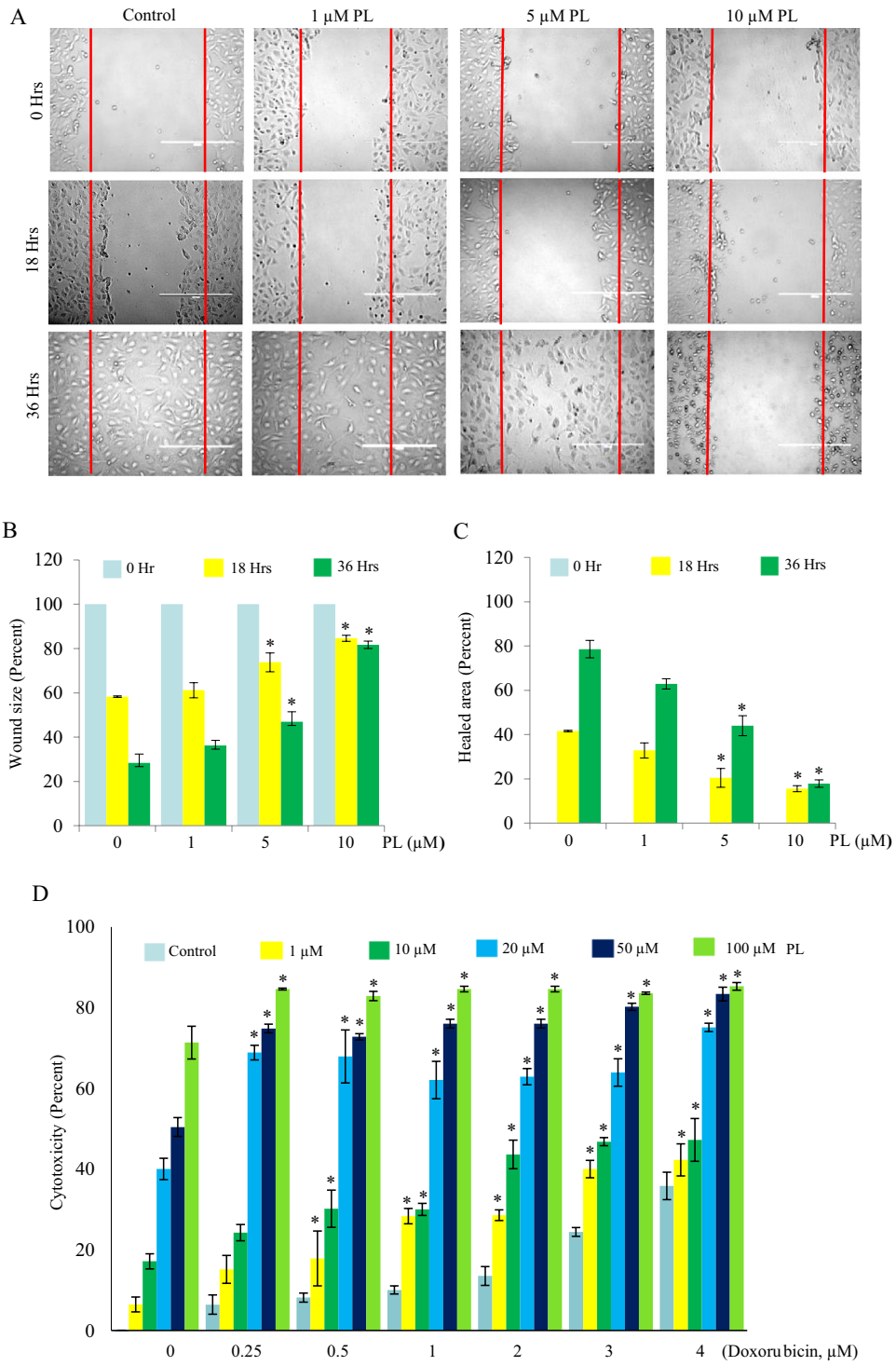


**Fig. 7** PL suppresses migration and enhances the efficacy of doxorubicin in breast cancer cells. **A** MDA-MB-231 cells were scratched at 90% confluency. Cells were then exposed with 1–10 µM PL and allowed to grow for 18–36 h. The size of the scratched area was determined and images were taken under the microscope. **B**, **C** The wound size and healed area (percent) was measured in the course of time. **D** MCF-7 cells were exposed with 1–100 µM PL for 24 h. After washing, the cells were exposed to 0.25–4 µM doxorubicin for another 24 h. The mitochondrial reductase activity was determined by measuring the optical density at 570 nm. The values indicate mean ± SE from three replicates. *indicate significance level as compared to the untreated group (**B–C**). The cytotoxicity was significantly increased (*) in cells treated with combination of two agents as compared to individual agent (**D**). $P < 0.05$. *PL* piperlongumine

treated with 10 µM PL. Overall, PL negatively affect the migration of breast cancer cells (Fig. 7C).

Although doxorubicin has been reported effective, acquisition of chemoresistance over time is a major obstacle. The ability of PL in sensitizing breast cancer cells to doxorubicin was evaluated. MCF-7 cells were exposed to 1–100 µM PL for 24 h. PL was then removed by washing and cells were treated with 0.25–4 µM doxorubicin for 24 h. For cytotoxcity, we measured the mitochondrial reductase activity. The cytotoxcity was significantly increased by the combination of two agents in comparison to single agent (Fig. 7D). For example, at 20 µM PL, 40% increase in the cytotoxicity was found in MCF-7 cells. Similarly, the cytotoxicity was increased at 8.2% by 0.5 µM doxorubicin. When the cells

were pre-treated with 20 µM PL before 0.5 µM doxorubicin, the cytotoxicity was observed at 68%. Overall, the sensitivity of breast cancer cells to doxorubicin is enhanced by PL.

Next, we examined whether the interaction between PL and doxorubicin is additive, synergistic or antagonistic by Chou-Talalay method [34]. We observed that PL induced cytotoxicity to a greater extent in MCF-7 cells when used in combination with doxorubicin (Supplementary Table 1). Since the interaction between PL and doxorubicin was found to be synergistic, we categorized the level of synergy into 5 different groups based on the value of CI (II) as shown in Supplementary Table 1. The values for CI index (II) indicated a very strong synergy in the group of cells treated with combinations of doxorubicin (0.25 µM, 0.5 µM, 1 µM, 2 µM, 3 µM, 4 µM) and the higher concentrations of PL (50 µM, 100 µM). The combination of doxorubicin with lower concentrations of PL (1 µM, 10 µM, 20 µM) produced slight to strong synergy (Supplementary Table 1).

## PL enhances the inhibitory effects of doxorubicin on mouse tumor growth

The observations discussed so far suggest that PL exhibit anticancer activities in cell lines. Before any drug can be tested in humans, its activity and safety should be thoroughly examined in animal models. Therefore, we examined if PL can suppress the growth of tumor in mice model implanted with ehrlich-lettre ascites carcinoma (EAC) cells. EAC cells were introduced under the mammary fat pad of mice. After 4 days, mice were randomized into 6 groups (Fig. 8A). In group I, the mice were administered with the vehicle. In groups II and IV, mice were provided with 10 mg and 20 mg PL per kg body weight, respectively (intraperitoneal, thrice per week). In groups III and V, mice were administered with doxorubicin at 1 mg and 2.5 mg per kg body weight, respectively (IP, twice per week). In group VI, the combination of two agents was provided to the mice [PL (10 mg per kg body weight): thrice per week + doxorubicin (1 mg per kg body weight): twice per week]. The mice were administered with the agent for 21 days. During the course of the treatment, the tumor volume, food intake and body weight was measured. At the end of the experiment, the tumor was removed, weighed and photographed. Both PL and doxorubicin were effective in reducing the tumor size. However, the combination of two agents drastically reduced the tumor size in comparison to individual agent. For example, on the last day of the experiment, the tumor volume was reduced by 44.2% and 19.9% in the group of mice administered with PL (10 mg/kg) and doxorubicin (1 mg/kg), respectively (Fig. 8B). However, when both agents were combined (PL: 10 mg/kg + doxorubicin: 1 mg/kg), 93.3% reduction in the tumor volume was observed on the last day of experiment (Fig. 8B). Further, the tumor volume was drastically increased over the course of treatment in the control group (Fig. 8B). Similarly, the weight of the tumor was also drastically reduced after the combination of two agents in comparison to individual agent (Fig. 8C). For example, the tumor weight was reduced by 29.8% and 20.3% in the mice group administered with 10 mg PL/kg and 1 mg DOXO/kg body weight, respectively. However, by combining two agents, the tumor weight was reduced by 84.9%. The difference in the actual tumor size on the last day of the experiment in different groups was obvious (Fig. 8D).

We also examined the effects of PL on the body weight of mice (Supplementary Fig S6A). A slight up and down in the total weight was observed over the course of treatment in the control group and at the lower concentration of PL (10 mg/kg body weight) and doxorubicin (1 mg/kg body weight). For example, the body weight was increased after 14 days in comparison to that observed after 7 days (Supplementary Fig S6A). Further, the body weight was decreased in these groups after 21 days in comparison to that observed after 14 days. However, almost similar values were observed in these group of mice after 21 days as that observed after 7 days. In the group of mice treated with PL (20 mg/kg body weight), doxorubicin (2.5 mg/kg body weight) and the combination of two agents (PL: 10 mg/kg + doxorubicin: 1 mg/kg), the body weight was increased over the course of treatment period. For instance, the body weight was increased after 14 days in comparison to that observed after 7 days. Similarly, the body weight was increased after 21 days in comparison to that observed after 14 days. The pattern of food intake by the mice in different groups was almost similar to that observed with the pattern of body weight (Supplementary Fig S6B).

We also examined the morphology of tumor from the control and PL treated mice. In the control group, the number of tumor cells were more in comparison to the treatment group (Supplementary Fig S7). Further, the nucleus to cytoplasm ratio in the untreated group was more in comparison to the experimental group. The nuclei were also disorganized and of variable shape in the control group. These features were restored in the tumor tissue from PL treated mice. Overall, these observations suggest the potency of PL in reducing mice tumor burden.

The rapidly dividing cancer cells are in increased demand of energy. An alteration in the lipid metabolism [51], and increased level of triglycerides and total cholesterol [52] are reported in cancer cells. We determined the effects of PL on the metabolic parameters of mice. The blood was collected from the control and PL-treated mice and the serum was separated. With an increase in the concentration of PL, the serum cholesterol and triglyceride levels were decreased (Fig. 8E, F). However, level of glucose was increased by increasing PL concentration (Fig. 8G).

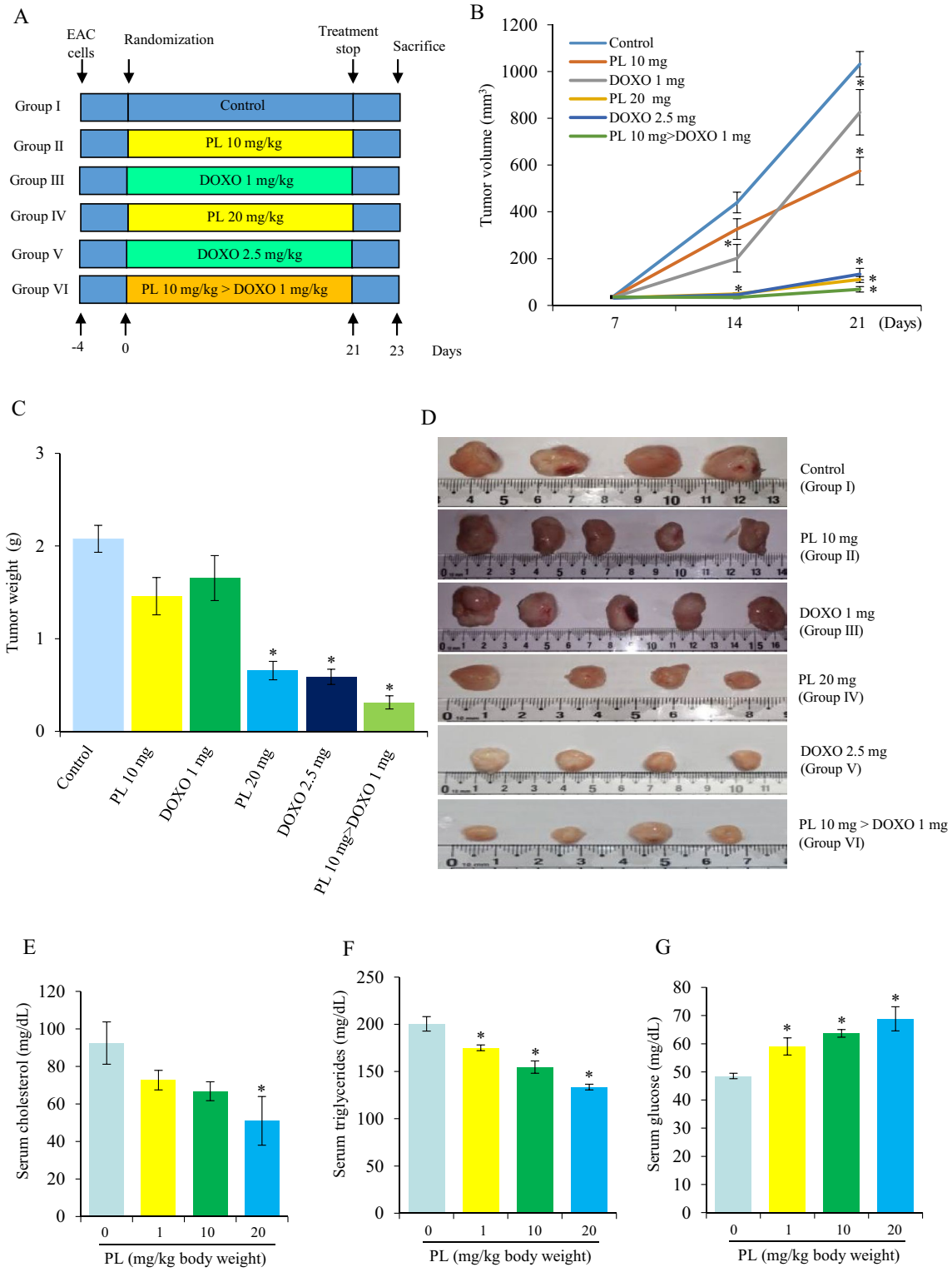


**Fig. 8** PL enhances the efficacy of doxorubicin in mouse model. **A** Outline of the experimental protocol. **B** Tumor volume was measured over the course of treatment period. **C** Tumor weight in various mice groups at the last day of the experiment. **D** An identification of actual tumors in various groups at the last day of the experiment as derived from mice. The levels of **E** cholesterol, **F** triglycerides, and **G** glucose in the serum was calculated using specific kit. Values shown are mean ± SE from 5 mice. *indicate the significance level as compared to untreated group ($P < 0.05$). *PL* piperlongumine, *DOXO* doxorubicin

## Discussion

Surgery, radiotherapy, chemotherapy and immunotherapy are preferred for breast cancer. These therapies have provided benefits to some cancer patients. However, the patients develop resistance mechanism over time. Moreover, these therapies produce several side effects in patients. The long pepper (source of PL) has been consumed since ancient time for a range of inflammatory diseases. PL was discovered in an effort to identify novel anti-cancer agents through a cell-based high-throughput screening approach. PL can selectively kill cancer cells while sparing non-malignant cells. The potential of this alkaloid in cancer models has been shown by previous studies [53]. The activity of this alkaloid has been demonstrated against cancer cell lines of diverse origin such as those of colon, lung, pancreatic, prostate, and renal [54]. However, the activities of this alkaloid in breast cancer and the underlying mechanism are poorly defined.

We used several breast cancer cell lines to examine PL's anti-cancer activities. The sensitivity of MDA-MB-231 cells to PL was more as compared to other cell lines. MCF-7 cell line is positive for ER- and PR-, and is categorised under the luminal A molecular subtype [55]. It is a non-invasive cell line with low metastatic potential [56]. On the other hand, MDA-MB-231 lack all three receptors (ER, PR, HER2) and thus belongs to the triple negative breast cancer (TNBC). Due to the absence of 3 receptors, TNBC is the most aggressive with poor prognosis [57]. Although the less aggressive breast cancer is relatively easy to control, the treatment of TNBC patients is challenging. In this context, the observations that MDA-MB-231 cells are more sensitive to PL is important. However, more studies using multiple TNBC cell lines are required before a definitive conclusion can be made.

The drug like properties of doxorubicin and PL was examined by in silico study. Although PL did not violate any of the Lipinski's rule, doxorubicin violated two rules. Pharmacokinetics analyses revealed that PL has better blood brain barrier and human intestinal permeability as compared to doxorubicin. The absence of carcinogenic and genotoxic activities further supports the drug like properties of PL. We observed that PL can enhance cytotoxicity in breast cancer cells. We used MTT assay that measures mitochondrial reductase activity as a function of cell viability. The mitochondrial reductase activity was suppressed by increasing PL concentration over a period of time. The long-term colony formation that mimics the in vivo situation further substantiated the observations of MTT assay. Whether 1–100 μM PL used in this study will be maintained for 24–72 h in vivo remains to be determined. In one study, the plasma concentrations of PL, post-administration (50 mg/kg) in rats, were found to be 1511.9 ng/mL, 418.2 ng/mL, and 41.9 ng/mL PL at 30 min, 3 h, and 24 h, respectively [58]. In another study, PL was found to enhance the bioavailability of docetaxel in Sprague–Dawley rats [59]. Contrary to this, PL has been reported to have limited bioavailability.

The anchorage independent growth assay confirmed the suppressive effects of PL on the tumor formation ability of the breast cancer cells. Employing multiple assays, we observed that the alkaloid triggered apoptosis in cancer cells. The AO/PI staining revealed the apoptosis inducing features such as membrane blebbing and chromatin condensation in PL treated cells. The changes in the nuclear structure, DNA laddering pattern and the cell cycle distribution in the PL treated cells further confirmed the apoptosis inducing potential of the alkaloid. The dissipation in the membrane potential suggests the involvement of mitochondria in the PL induced apoptosis. We observed fragmentation in the mitochondria in the group of cells treated with PL. The fission in the mitochondria has been reported to participate in Bax-mediated permeabilization of the outer mitochondrial membrane and cytochrome c release, which is a feature of apoptosis [60]. Consistent with this report, PL was found to induce cytochrome c release into the cytosol. The invasion and metastasis are the substantial cause of breast cancer related death. Before metastasis, cancer cells undergo migration and invasion. The negative effects of PL on migration of MDA-MB-231 cells may also lead to a suppression in metastasis.

A variety of mechanisms has been proposed for the anti-cancer activities of PL. More specifically, the agent has been shown to induce caspase activation, ERK activation, and to modulate the expression of cancer related proteins such as cell division cycle-2 (cdc-2), cyclin-dependent kinase2 (cdk2), cyclin D1, Bcl-2, Raf-1, survivin, VEGF, cluster of differentiation 31 (CD31), HIF-2, and Twist. PL-induced apoptosis may involve reduction of MYC, NF-κB, and Epstein-barr virus latent membrane protein 1 (LMP-1) in Burkitt lymphoma [61]. PL can also suppress NF-κB activity in leukemia, multiple myeloma and prostate cancer cells. Whether PL reduces NF-κB activity in breast cancer is not known. Our observations revealed the negative role of PL on inducible NF-κB activation in breast cancer cells. Employing molecular docking tools, we observed that PL can bind with the proteins in the NF-κB pathway including p65 and p50. Because NF-κB regulate numerous downstream cancer related genes including crucial tumorigenic proteins, this transcription factor is believed to be master regulator of tumor development [10]. How PL inhibit NF-κB activation was not investigated. PL has been reported to reduce NF-κB activation by direct binding to $Cys^{179}$ of IKKβ [27]. $Cys^{179}$ is a redox-sensitive amino acid, which constitute the IKK catalytic subunits. Although multiple proteins are involved in the NF-κB signalling [62], PL inhibits NF-κB by modifying

$Cys^{179}$ in the IKKβ activation loop. The similar effects on $Cys^{179}$ has been reported by nimbolide [63] and butein [64]. It is possible that PL directly bind to IKK in breast cancer cells for inhibiting NF-κB activation. We also observed a dysregulation in lncRNAs in breast cancer cells by PL. Recent studies suggest that lncRNA and NF-κB signalling cross-talk in human diseases including cancer. Whether the dysregulation in lncRNAs expression is a cause or consequence of NF-κB inactivation remains to be examined.

PL induced ROS level in breast cancer cells. Previous studies have also reported the ROS inducing potential of PL in multiple cancer cells such as colorectal cancer [9], hepatocellular carcinoma [19], NSCLC [22], and pancreatic cancer cells [65]. Various other small molecules can elevate ROS levels and induce cancer cell death [66]. The small molecules have also demonstrated a degree of selectivity towards cancer cells. It is to be noted that for measuring ROS level, the cells were stained with DCFDA after treatment with PL for 1 h. The changes in ROS generation due to long-persisting effects of PL due to perturbed mitochondria cannot be ruled out.

PL, at a relatively lower concentrations (10 and 20 mg/kg) was found to suppress tumor growth in mouse model. In a previous report, PL (2.5 mg/kg) did not produce significant effect in human colorectal cancer xenograft model [67]. Similarly, an insignificant change in the tumor growth was observed in a gastric cancer xenograft mice model by PL at 4 mg/kg [19]. In mice model bearing sarcoma 180 cells, PL (25 mg/kg, 50 mg/kg) significantly reduced the tumor volume. Further, the nano-emulsions of PL was associated with enhanced bioavailability and efficacy [68]. Doxorubicin, an anthracycline has demonstrated potential in breast cancer patients. However, cancer cells develop resistance to doxorubicin over time due to multiple mechanisms, the dominant of which is the presence of P-glycoprotein (PGP). PGP is the classic multidrug resistance (MDR) phenotype [69]. The dysregulation in the NF-κB and lncRNAs siganling also contribute to the drug resistance. We observed that PL potentiated the effects of doxorubicin in cancer cell lines and in mice model. Similar to our observations, PL was found to radiosensitize the colorectal cancer cells [9]. PL was also found to synergize with doxorubicin in its activity against prostate cancer through mediation of carbonyl reductase 1 [70]. Consistent with this report, we observed a varied level of synergy between doxorubicin and PL. We observed that the body weight and the food intake by the mice in vehicle control, PL treated mice (10 mg/kg), and doxorubicin treated mice (1 mg/kg) was reduced after 21 days in comparison to that observed after 14 days. Conversely, an improvement in the food intake and body weight was found in the group of mice administered with PL (20 mg/kg), doxorubicin (2.5 mg/kg) and the combination of two agents. As the disease progresses, the cancer patients develop several associated problems such as anorexia, cachexia, depression and fatigue [71]. An improvement in the body weight and food intake by the PL and PL + doxorubicin further suggests the benefits of this alkaloid for cancer patients. Similar to our observations, genistein was found to reduce anorexia in rats [72].

Because of preferential use of aerobic glycolysis (Warburg effect), breast cancer cells like other solid tumors heavily depend on GLUT1. Widely distributed in normal tissue, GLUT1 is overexpressed in multiple tumor types. GLUT1 can enhance the aggressiveness of breast cancer [73]. The treatment of cells with PL was associated with an accumulation of extracellular glucose and an increase in the extracellular pH towards alkaline range. These observations suggest that PL impaired the glucose import in breast cancer cells. This may result in the induction of cell death due to glucose deprivation. Similar to our observations, fasentine, genistein, ritonavir and STF13 are known to exhibit anti-cancer activities by targeting GLUT1, inhibiting glucose import, leading to cell death through glucose deprivation [74]. The agents derived from Mother Nature such as cryptocaryone [75] and resveratrol [76] can also inhibit glucose import either by direct binding to GLUT1 or in an indirect manner. GLUT1 can also cross talk with NF-κB and lncRNAs [15]. A possibility that the multitargeting by PL on these signalling molecules contribute to its anti-cancer and chemosensitization activities cannot be ruled out.

Overall, the results suggest the potential of PL for breast cancer treatment. PL can suppress tumor development both in vitro and in vivo (Supplementary Fig S8). Further, PL enhances the efficacy of doxorubicin for breast cancer. The most likely mechanism for its anticancer activities is through modulation of NF-κB, lncRNAs and generation of ROS. PL can also modulate metabolic parameters in EAC mice model. EAC cells used in this study have limitations as they do not accurately mimic the breast cancer. The observations from tumor bearing mice model may or may not reflect what would actually occur with breast cancer cell lines. More studies are required before PL can be recommended for human clinical trials for breast cancer.

**Supplementary Information** The online version contains supplementary material available at https://doi.org/10.1007/s10495-022-01711-6.

**Acknowledgements** The study was supported in part from Indian Council of Medical Research, New Delhi (5/13/51/2020/NCD-III) and Science and Engineering Research Board, New Delhi (ECR/2016/000034). NA (5/3/8/40/ITR-F/2019-ITR), VR (3/2/2/43/2018/Online Onco Fship/NCD-III), and SM (3/1/3/JRF-2016/LS/HRD-65-80388) received fellowship from Indian Council of Medical Research, New Delhi. SSV was supported from DBT New Delhi (DBT/2017/BHU/786). AS was supported from UGC New Delhi [No.F.82-1/2018(SA-III)]. We thankfully acknowledge the support

from Dr. Rahul K. Singh, Department of Zoology, BHU and Dr. P.K. Nayak, Department of Pharmaceutics Engineering and Technology, IIT BHU with Chemi-Doc system and animal house facility, respectively. The analyses with real-time PCR system and flow cytometer were performed at BHU's Interdisciplinary School of Life Sciences.

## References

1. Hanahan D, Weinberg RA (2011) Hallmarks of cancer: the next generation. Cell 144:646–674
2. Zaid H, Antonescu CN, Randhawa VK, Klip A (2008) Insulin action on glucose transporters through molecular switches, tracks and tethers. Biochem J 413:201–215
3. Younes M, Brown R, Mody D, Fernandez L, Laucirica R (1995) GLUT1 expression in human breast carcinoma: correlation with known prognostic markers. Anticancer Res 15:2895–2898
4. Bisetto S, Whitaker-Menezes D, Wilski NA et al (2018) Monocarboxylate transporter 4 (MCT4) knockout mice have attenuated 4NQO induced carcinogenesis; a role for MCT4 in Driving oral squamous cell cancer. Front Oncol 8:324
5. Vaughan RA, Garcia-Smith R, Dorsey J, Griffith JK, Bisoffi M, Trujillo KA (2013) Tumor necrosis factor alpha induces Warburg-like metabolism and is reversed by anti-inflammatory curcumin in breast epithelial cells. Int J Cancer 133:2504–2510
6. Sommermann TG, O'Neill K, Plas DR, Cahir-McFarland E (2011) IKKβ and NF-κB transcription govern lymphoma cell survival through AKT-induced plasma membrane trafficking of GLUT1. Can Res 71:7291–7300
7. Mauro C, Leow SC, Anso E et al (2011) NF-κB controls energy homeostasis and metabolic adaptation by upregulating mitochondrial respiration. Nat Cell Biol 13:1272–1279
8. Liu J, Zhang C, Wu R et al (2015) RRAD inhibits the Warburg effect through negative regulation of the NF-κB signaling. Oncotarget 6:14982
9. Wang H, Jiang H, Corbet C et al (2019) Piperlongumine increases sensitivity of colorectal cancer cells to radiation: involvement of ROS production via dual inhibition of glutathione and thioredoxin systems. Cancer Lett 450:42–52
10. Gupta SC, Sundaram C, Reuter S, Aggarwal BB (2010) Inhibiting NF-κB activation by small molecules as a therapeutic strategy. Biochim et Biophys Acta (BBA) 1799:775–787
11. Gupta SC, Awasthee N, Rai V, Chava S, Gunda V, Challagundla KB (2019) Long non-coding RNAs and nuclear factor-B crosstalk in cancer and other human diseases. Biochim et Biophys Acta (BBA) 1873:188316
12. Liu Y, He X, Chen Y, Cao D (2020) Long non-coding RNA LINC00504 regulates the Warburg effect in ovarian cancer through inhibition of miR-1244. Mol Cell Biochem 464:39–50
13. Malakar P, Stein I, Saragovi A et al (2019) Long noncoding RNA MALAT1 regulates cancer glucose metabolism by enhancing mTOR-mediated translation of TCF7L2. Can Res 79:2480–2493
14. Xiang S, Gu H, Jin L, Thorne RF, Zhang XD, Wu M (2018) LncRNA IDH1-AS1 links the functions of c-Myc and HIF1α via IDH1 to regulate the Warburg effect. Proc Natl Acad Sci 115:E1465–E1474
15. Liu X, Gan B (2016) lncRNA NBR2 modulates cancer cell sensitivity to phenformin through GLUT1. Cell Cycle 15:3471–3481
16. Bezerra DP, Pessoa C, de Moraes MO, Saker-Neto N, Silveira ER, Costa-Lotufo LV (2013) Overview of the therapeutic potential of piplartine (piperlongumine). Eur J Pharm Sci 48:453–463
17. Costa-Lotufo LV, Montenegro RC, Alves APN et al (2010) The contribution of natural products as source of new anticancer drugs: Studies carried out at the national experimental oncology laboratory from the Federal University of Ceará. Revista Virtual de Química 2:47–58
18. Chen SY, Huang HY, Lin HP, Fang CY (2019) Piperlongumine induces autophagy in biliary cancer cells via reactive oxygen species-activated Erk signaling pathway. Int J Mol Med 44:1687–1696
19. Zhang P, Shi L, Zhang T et al (2019) Piperlongumine potentiates the antitumor efficacy of oxaliplatin through ROS induction in gastric cancer cells. Cell Oncol 42:847–860
20. Randhawa H, Kibble K, Zeng H, Moyer M, Reindl K (2013) Activation of ERK signaling and induction of colon cancer cell death by piperlongumine. Toxicol In Vitro 27:1626–1633
21. Yao Y, Sun Y, Shi M et al (2016) Piperlongumine induces apoptosis and reduces bortezomib resistance by inhibiting STAT3 in multiple myeloma cells. Oncotarget 7:73497
22. Li Q, Chen L, Dong Z et al (2019) Piperlongumine analogue L50377 induces pyroptosis via ROS mediated NF-κB suppression in non-small-cell lung cancer. Chem-Biol interact 313:108820
23. Dhillon H, Chikara S, Reindl KM (2014) Piperlongumine induces pancreatic cancer cell death by enhancing reactive oxygen species and DNA damage. Toxicol Rep 1:309–318
24. Chen S-Y, Liu G-H, Chao W-Y et al (2016) Piperlongumine suppresses proliferation of human oral squamous cell carcinoma through cell cycle arrest, apoptosis and senescence. Int J Mol Sci 17:616
25. Kong E-H, Kim Y-J, Kim Y-J et al (2008) Piplartine induces caspase-mediated apoptosis in PC-3 human prostate cancer cells. Oncol Rep 20:785–792
26. Wang F, Mao Y, You Q, Hua D, Cai D (2015) Piperlongumine induces apoptosis and autophagy in human lung cancer cells through inhibition of PI3K/Akt/mTOR pathway. Int J Immunopathol Pharmacol 28:362–373
27. Han JG, Gupta SC, Prasad S, Aggarwal BB (2014) Piperlongumine chemosensitizes tumor cells through interaction with cysteine 179 of IκBα kinase, leading to suppression of NF-κB–regulated gene products. Mol Cancer Ther 13:2422–2435
28. Fofaria NM, Srivastava SK (2014) Critical role of STAT3 in melanoma metastasis through anoikis resistance. Oncotarget 5:7051
29. Xiong X-x, Liu J-m, Qiu X-y, Pan F, Yu S-b, Chen X-q (2015) Piperlongumine induces apoptotic and autophagic death of the primary myeloid leukemia cells from patients via activation of ROS-p38/JNK pathways. Acta Pharmacol Sin 36:362–374
30. Thongsom S, Suginta W, Lee KJ, Choe H, Talabnin C (2017) Piperlongumine induces G2/M phase arrest and apoptosis in cholangiocarcinoma cells through the ROS-JNK-ERK signaling pathway. Apoptosis 22:1473–1484
31. Chen Y, Liu JM, Xiong XX et al (2015) Piperlongumine selectively kills hepatocellular carcinoma cells and preferentially inhibits their invasion via ROS-ER-MAPKs-CHOP. Oncotarget 6:6406
32. Yao J-X, Yao Z-F, Li Z-F, Liu Y-B (2014) Radio-sensitization by Piper longumine of human breast adenoma MDA-MB-231 cells in vitro. Asian Pac J Cancer Prev 15:3211–3217
33. Verma SS, Rai V, Awasthee N et al (2019) Isodeoxyelephantopin, a sesquiterpene lactone induces ROS generation, suppresses NF-κB activation, modulates LncRNA expression and exhibit activities against breast cancer. Sci Rep 9:1–16
34. Chou TC (2010) Drug combination studies and their synergy quantification using the Chou-Talalay method. Cancer Res 70:440–446
35. Gupta SC, Prasad S, Sethumadhavan DR, Nair MS, Mo Y-Y, Aggarwal BB (2013) Nimbolide, a limonoid triterpene, inhibits growth of human colorectal cancer xenografts by suppressing the proinflammatory microenvironment. Clin Cancer Res 19:4465–4476

36. Awasthee N, Rai V, Verma SS, Francis KS, Nair MS, Gupta SC (2018) Anti-cancer activities of Bharangin against breast cancer: Evidence for the role of NF-κB and lncRNAs. Biochim et Biophys Acta (BBA) 1862:2738–2749
37. Zhao Y-R, Li H-M, Zhu M et al (2018) Non-benzoquinone geldanamycin analog, WK-88-1, induces apoptosis in human breast cancer cell lines. J Microbiol Biotechnol 28:542–550
38. Saeed U, Durgadoss L, Valli RK, Joshi DC, Joshi PG, Ravindranath V (2008) Knockdown of cytosolic glutaredoxin 1 leads to loss of mitochondrial membrane potential: implication in neurodegenerative diseases. PLoS ONE 3:e2459
39. Gupta SC, Singh R, Asters M et al (2016) Regulation of breast tumorigenesis through acid sensors. Oncogene 35:4102–4111
40. Gupta SC, Singh R, Pochampally R, Watabe K, Mo Y-Y (2014) Acidosis promotes invasiveness of breast cancer cells through ROS-AKT-NF-κB pathway. Oncotarget 5:12070
41. Thang ND, Yajima I, Kumasaka MY et al (2011) Barium promotes anchorage-independent growth and invasion of human HaCaT keratinocytes via activation of c-SRC kinase. PLoS ONE 6:e25636
42. Mishra S, Verma SS, Rai V et al (2019) Curcuma raktakanda induces apoptosis and suppresses migration in cancer cells: role of reactive oxygen species. Biomolecules 9:159
43. Schmittgen TD, Livak KJ (2008) Analyzing real-time PCR data by the comparative C T method. Nat Protoc 3:1101
44. Cheng F, Li W, Zhou Y et al (2012) admetSAR: a comprehensive source and free tool for assessment of chemical ADMET properties. ACS Publications, Washington DC
45. Lipinski CA, Lombardo F, Dominy BW, Feeney PJ (2001) Experimental and computational approaches to estimate solubility and permeability in drug discovery and development settings. Adv Drug Deliv Rev 46:3–26
46. Morris GM, Huey R, Lindstrom W et al (2009) AutoDock4 and AutoDockTools4: automated docking with selective receptor flexibility. J Comput Chem 30:2785–2791
47. Pierce BG, Hourai Y, Weng Z (2011) Accelerating protein docking in ZDOCK using an advanced 3D convolution library. PLoS ONE 6:e24657
48. Ozaslan M, Karagoz ID, Kilic IH, Guldur ME (2011) Ehrlich ascites carcinoma. Afr J Biotech 10:2375–2378
49. Tomayko MM, Reynolds CP (1989) Determination of subcutaneous tumor size in athymic (nude) mice. Cancer Chemother Pharmacol 24:148–154
50. Ranjan A, Choubey M, Yada T, Krishna A (2019) Direct effects of neuropeptide nesfatin-1 on testicular spermatogenesis and steroidogenesis of the adult mice. Gen Comp Endocrinol 271:49–60
51. Long J, Zhang C-J, Zhu N et al (2018) Lipid metabolism and carcinogenesis, cancer development. Am J Cancer Res 8:778
52. Lofterød T, Mortensen ES, Nalwoga H et al (2018) Impact of pre-diagnostic triglycerides and HDL-cholesterol on breast cancer recurrence and survival by breast cancer subtypes. BMC Cancer 18:1–11
53. Bezerra DP, Militão GCG, De Castro FO et al (2007) Piplartine induces inhibition of leukemia cell proliferation triggering both apoptosis and necrosis pathways. Toxicol In Vitro 21:1–8
54. Bezerra DP, Castro FOd, Alves APN et al (2008) In vitro and in vivo antitumor effect of 5-FU combined with piplartine and piperine. J Appl Toxicol 28:156–163
55. Done S (2011) Breast cancer: recent advances in biology, imaging and therapeutics. BoD-Books on Demand, Hamburg
56. Shirazi FH, Zarghi A, Kobarfard F et al (2011) Remarks in successful cellular investigations for fighting breast cancer using novel synthetic compounds. In: Gunduz M, Gunduz E (eds) Breast cancer: focusing tumor microenvironment, stem cells and metastasis. BoD-Books on Demand, Hamburg, pp 85–102
57. Anders C, Carey LA (2008) Understanding and treating triple-negative breast cancer. Oncology (Williston Park) 22:1233
58. Bezerra DP, Pessoa C, Moraes MO et al (2012) Sensitive method for determination of piplartine, an alkaloid amide from piper species, in rat plasma samples by liquid chromatography-tandem mass spectrometry. Quim Nova 35:460–465
59. Patel K, Chowdhury N, Doddapaneni R, Boakye CHA, Godugu C, Singh M (2015) Piperlongumine for enhancing oral bioavailability and cytotoxicity of docetaxel in triple-negative breast cancer. J Pharm Sci 104:4417–4426
60. Tanaka A, Youle RJ (2008) A chemical inhibitor of DRP1 uncouples mitochondrial fission and apoptosis. Mol Cell 29:409–410
61. Han S-S, Son D-J, Yun H, Kamberos NL, Janz S (2013) Piperlongumine inhibits proliferation and survival of Burkitt lymphoma in vitro. Leuk Res 37:146–154
62. Rothwarf DM, Karin M (1999) The NF-κB activation pathway: a paradigm in information transfer from membrane to nucleus. Sci STKE 1999:re1
63. Gupta SC, Prasad S, Reuter S et al (2010) Modification of cysteine 179 of IκBα kinase by nimbolide leads to down-regulation of NF-κB-regulated cell survival and proliferative proteins and sensitization of tumor cells to chemotherapeutic agents. J Biol Chem 285:35406–35417
64. Pandey MK, Gupta SC, Nabavizadeh A, Aggarwal BB (2017) Regulation of cell signaling pathways by dietary agents for cancer prevention and treatment. Semin Cancer Biol 46:158–181
65. Mohammad J, Dhillon H, Chikara S et al (2018) Piperlongumine potentiates the effects of gemcitabine in in vitro and in vivo human pancreatic cancer models. Oncotarget 9:10457
66. Wondrak GT (2009) Redox-directed cancer therapeutics: molecular mechanisms and opportunities. Antioxid Redox Signal 11:3013–3069
67. Chen W, Lian W, Yuan Y, Li M (2019) The synergistic effects of oxaliplatin and piperlongumine on colorectal cancer are mediated by oxidative stress. Cell Death Dis 10:1–12
68. Fofaria NM, Qhattal HSS, Liu X, Srivastava SK (2016) Nanoemulsion formulations for anti-cancer agent piplartine: characterization, toxicological, pharmacokinetics and efficacy studies. Int J Pharm 498:12–22
69. Nielsen D, Maare C, Skovsgaard T (1996) Cellular resistance to anthracyclines. Gen Pharmacol 27:251–255
70. Piska K, Koczurkiewicz P, Wnuk D et al (2019) Synergistic anticancer activity of doxorubicin and piperlongumine on DU-145 prostate cancer cells: the involvement of carbonyl reductase 1 inhibition. Chem-Biol Interact 300:40–48
71. Gupta SC, Kim JH, Kannappan R, Reuter S, Dougherty PM, Aggarwal BB (2011) Role of nuclear factor-κ B-mediated inflammatory pathways in cancer-related symptoms and their regulation by nutritional agents. Exp Biol Med 236:658–671
72. Tsushima H, Mori M (2001) Involvement of protein kinase C and tyrosine kinase in lipopolysaccharide-induced anorexia. Pharmacol Biochem Behav 69:17–22
73. Brown RS, Wahl RL (1993) Overexpression of glut-1 glucose transporter in human breast cancer an immunohistochemical study. Cancer 72:2979–2985
74. Chan DA, Sutphin PD, Nguyen P et al (2011) Targeting GLUT1 and the Warburg effect in renal cell carcinoma by chemical synthetic lethality. Sci Transl Med 3:94ra70
75. Kurniadewi F, Juliawaty LD, Syah YM et al (2010) Phenolic compounds from Cryptocarya konishii: their cytotoxic and tyrosine kinase inhibitory properties. J Nat Med 64:121–125
76. Vetterli L, Brun T, Giovannoni L, Bosco D, Maechler P (2011) Resveratrol potentiates glucose-stimulated insulin secretion in INS-1E β-cells and human islets through a SIRT1-dependent mechanism. J Biol Chem 286:6049–6060